2018

The Genome of Austrofundulus Limnaeus Offers Insights into Extreme Vertebrate Stress Tolerance and Embryonic Development

Josiah Tad Wagner
Portland State University, jtwagn@gmail.com

Param Priya Singh
Stanford University

Amie L. Romney
Portland State University, arom2@pdx.edu

Claire L. Riggs
Portland State University, rclaire@pdx.edu

Patrick Minx
Washington University School of Medicine in St. Louis

Follow this and additional works at: https://pdxscholar.library.pdx.edu/clee_pubs

See next page for additional authors

Part of the Biology Commons, Genetics Commons, and the Genomics Commons

Let us know how access to this document benefits you.

Citation Details

Wagner, Josiah T., Param Priya Singh, Amie L. Romney, Claire L. Riggs, Patrick Minx, Steven C. Woll, Jake Roush, Wesley C. Warren, Anne Brunet, and Jason E. Podrabsky. "The genome of Austrofundulus limnaeus offers insights into extreme vertebrate stress tolerance and embryonic development." BMC genomics 19, no. 1 (2018): 155.

Authors

Josiah Tad Wagner, Param Priya Singh, Amie L. Romney, Claire L. Riggs, Patrick Minx, Steven Cody Woll, Jake Roush, Wesley C. Warren, Anne Brunet, and Jason E. Podrabsky

BMC Genomics

CrossMark

The genome of *Austrofundulus limnaeus* offers insights into extreme vertebrate stress tolerance and embryonic development

Josiah T. Wagner[1,5*], Param Priya Singh[2], Amie L. Romney[1], Claire L. Riggs[1], Patrick Minx[3], Steven C. Woll[1], Jake Roush[1], Wesley C. Warren[3], Anne Brunet[2,4] and Jason E. Podrabsky[1]

Abstract

Background: The annual killifish *Austrofundulus limnaeus* inhabits ephemeral ponds in northern Venezuela, South America, and is an emerging extremophile model for vertebrate diapause, stress tolerance, and evolution. Embryos of *A. limnaeus* regularly experience extended periods of desiccation and anoxia as a part of their natural history and have unique metabolic and developmental adaptations. Currently, there are limited genomic resources available for gene expression and evolutionary studies that can take advantage of *A. limnaeus* as a unique model system.

Results: We describe the first draft genome sequence of *A. limnaeus*. The genome was assembled de novo using a merged assembly strategy and was annotated using the NCBI Eukaryotic Annotation Pipeline. We show that the assembled genome has a high degree of completeness in genic regions that is on par with several other teleost genomes. Using RNA-seq and phylogenetic-based approaches, we identify several candidate genes that may be important for embryonic stress tolerance and post-diapause development in *A. limnaeus*. Several of these genes include heat shock proteins that have unique expression patterns in *A. limnaeus* embryos and at least one of these may be under positive selection.

Conclusion: The *A. limnaeus* genome is the first South American annual killifish genome made publicly available. This genome will be a valuable resource for comparative genomics to determine the genetic and evolutionary mechanisms that support the unique biology of annual killifishes. In a broader context, this genome will be a valuable tool for exploring genome-environment interactions and their impacts on vertebrate physiology and evolution.

Keywords: Annual killifish, Stress tolerance, Transcriptome, Gene expression, Fish genome, Positive selection, *Austrofundulus limnaeus*, Development

Background

All vertebrates require oxygen and water to complete their life cycles. However, environments are not always forgiving when it comes to constantly providing these basic needs for life. Many metazoans that thrive in highly stressful or variable environments cope by arresting development and entering into states of metabolic depression [1–8]. Examples of organisms able to cope with high environmental stress conditions are typically prokaryotes and invertebrates; extremophile vertebrates are relatively rare. The annual killifish *Austrofundulus limnaeus* (Schultz 1949) is one of the best-described extremophile vertebrates and its embryos have been shown to tolerate low to no oxygen, high and low salinity, ultraviolet-C radiation exposure, and desiccation [9–12]. This stress-tolerant phenotype is essential for survival in tropical and subtropical ephemeral ponds

* Correspondence: wagnejos@ohsu.edu
[1]Department of Biology, Center for Life in Extreme Environments, Portland State University, Portland, Oregon, USA
[5]Knight Cancer Early Detection Advanced Research Center, Oregon Health and Science University, Portland, Oregon, USA
Full list of author information is available at the end of the article

Wagner *et al. BMC Genomics* (2018) 19:155

Page 2 of 21

that experience periods of daily temperature fluctuations, seasonal habitat desiccation, anoxia, and hypoxia [13, 14]. Because adult annual killifishes are unable to endure the dry season, populations persist due to the survival of drought-tolerant embryos that can depress metabolism in a state of suspended animation, known as diapause [7, 9]. Diapause may occur at three distinct stages of development in annual killifishes, termed diapause I, II, and III [15–17]. Diapause I (DI) can occur early in development after completion of epiboly but prior to the formation of the embryonic axis. Contrasting with the typical pattern of convergence and extension of the amoeboid (deep) embryonic blastomeres that is observed in most other teleost embryos during epiboly, deep blastomeres of *A. limnaeus* dissociate and migrate away from each other across the yolk surface during epiboly [18, 19]. Essentially, this process appears to temporally disconnect epiboly from germ layer formation in annual killifishes and these deep cells can remain dispersed across the yolk surface for several days before reaggregating and forming a definitive embryonic axis [16]. Although the biological significance and mechanism of this phenomenon are still unclear, it has been suggested that the spatial arrangement of embryonic cells in DI may allow damaged cells to be "sloughed" and replaced by surrounding pluripotent cells [12, 16]. This phenomenon may be facilitated by unique expression of genes important for gastrulation [20]. Diapause II (DII) occurs in the long-somite embryo approximately midway through development, just prior to the major phases of organogenesis, and appears to be the most stress-resistant diapause stage [15, 17, 21]. Finally, embryos can arrest as a late pre-hatching embryo in diapause III (DIII) rather than immediately hatching [17, 22]. While the majority of *A. limnaeus* embryos will enter into DII, a small proportion of "escape" embryos will bypass DII and instead develop directly to DIII or hatching [17, 23]. Importantly, entrance into diapause is an alternative developmental trajectory that is unique biochemically, physiologically, and morphologically from escape embryos.

The unique biology of *A. limnaeus* and other annual killifishes provides an exceptional opportunity to study questions related to stress physiology, development, and evolution by making comparisons within species and across species [2, 21, 24]. One of the best-studied examples of *A. limnaeus* as an important and unique model organism stems from the extreme anoxia tolerance of its embryos, having the highest known tolerance compared to any other vertebrate after temperature is considered [11]. In contrast, insufficient oxygen quickly leads to disruption of cellular homeostasis and cell death in mammals during similar developmental stages, and especially in adult mammalian tissues [25, 26]. This tolerance in *A. limnaeus* embryos peaks at DII (LD$_{50}$ anoxia = 65 days)
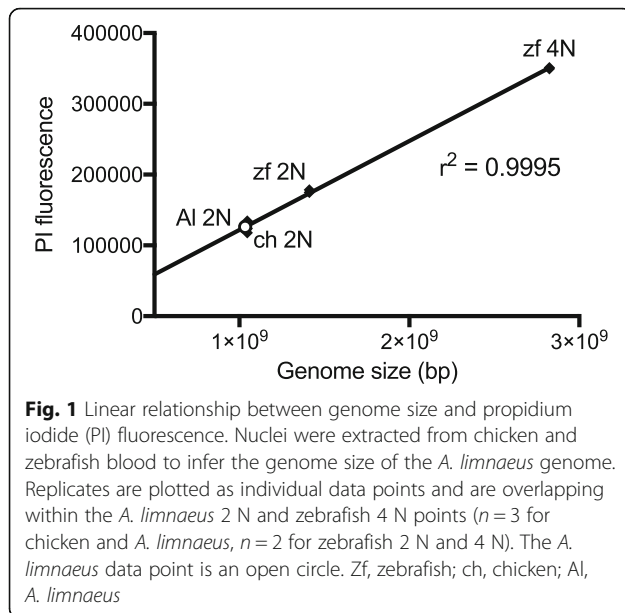
and is retained for up to 4 days post-diapause (dpd) [11]. Importantly, 4 dpd embryos are physiologically and developmentally distinct from DII embryos, as they have reentered the cell cycle and are metabolically active, and therefore are a model that can have broader implications for comparative studies to other vertebrates. Although the metabolic and cell cycle mechanisms that may support extreme anoxia tolerance and post-DII (PDII) development have previously been explored [11, 27–29], a comprehensive study of the genetic, evolutionary, and gene expression mechanisms that may support the unique features of *A. limnaeus* and other annual killifishes has yet to be performed. Recent work on the African annual killifish, *Nothobranchius furzeri*, suggests that positive selection on *N. furzeri* genes may have a role in determining the annual killifish phenotype [30, 31]. Because it has long been hypothesized that annualism was evolved independently several times within the killifish families Rivulidae and Nothobranchidae [32–34], determining if the evolutionary mechanisms are shared between different annual killifish lineages will have broad implications for the understanding of complex phenotype evolution.

The development of an *A. limnaeus* genomics resource is essential for understanding the evolutionary background of its unique phenotype, and is a necessary tool for functional research such as RNA-seq based expression studies. In this work we present the first de novo draft genome assembly and annotation of a lab reared *A. limnaeus* individual originating from a population near the town of Quisiro, in the Maracaibo Basin of Venezuela [35]. This population has been bred under laboratory conditions since 1995 and is currently maintained at the Center for Life in Extreme Environments Aquatics Facility, Portland State University, Portland, OR. We show for the first time the gene expression profiles that support extreme anoxia tolerance and post-diapause development, as well as potential genes under positive selection in the *A. limnaeus* lineage compared to several teleost species. The resulting genome and annotation is the first publicly available representative of a South American annual killifish and we discuss several genes of interest for future studies in stress tolerance and vertebrate development.

Results
Estimation of genome size
Flow cytometry quantification of propidium iodide fluorescence intensity yields an estimated genome size for *A. limnaeus* of 1.03 Gbp when *Danio rerio* (zebrafish) and *Gallus gallus* (domestic chicken) free-nuclei were used as standards (Fig. 1). *A. limnaeus* genome size was also estimated by k-mer frequency in Allpaths-LG [36]. This

Wagner *et al. BMC Genomics* (2018) 19:155

Page 3 of 21

Fig. 1 Linear relationship between genome size and propidium iodide (PI) fluorescence. Nuclei were extracted from chicken and zebrafish blood to infer the genome size of the *A. limnaeus* genome. Replicates are plotted as individual data points and are overlapping within the *A. limnaeus* 2 N and zebrafish 4 N points (*n* = 3 for chicken and *A. limnaeus*, *n* = 2 for zebrafish 2 N and 4 N). The *A. limnaeus* data point is an open circle. Zf, zebrafish; ch, chicken; Al, *A. limnaeus*

Table 2 Genome assembly metrics for the *A. limnaeus* genome version 1.0

Metric	Length/number
Total sequence length	866,963,281 bp
Total assembly gap length	171,917,903 bp
Number of scaffolds	29,785
Scaffold N50	1,098,383 bp
Scaffold L50	184 bp
Number of contigs	168,369
Contig N50	8097 bp
Contig L50	24,012 bp

sequence-based method estimated the genome at 974 Mbp, about 5% smaller than the flow cytometry estimate (Table 1).

Genome assembly and annotation results

To provide a high-quality genome for annotation, we used a merged assembly strategy that utilized mate-pair libraries for scaffolding. Of the initial read pool used as input for Allpaths-LG, the assembler used 65.6% and 28.6% of the fragment and jumping libraries, respectively, for the initial assembly of the *A. limnaeus* genome at a sequencing coverage of 94X. This Allpaths-LG assembly produced 141,049 contigs longer than 1000 bp, and within these contigs 650 Mbp was assembled. JR-assembler assembled 370,267 contigs (> 500 bp) with an N50 of 1.3 kbp and a total assembled length of 433 Mbp. After merging the two assembles with a graph accordance assembly program [37], the *A. limnaeus* draft genome assembly v1.0 has 168,369 contigs, has a contig N50 of 8.1 kb, and is 695 Mbp in total length. Use of mate-pair libraries for scaffolding with SSPACE

organized contigs into 29,785 scaffolds, with an N50 of 1.1 Mbp, and increased the total sequence length to 867 Mbp, including gaps (Table 2). Based on the results of our genome size estimates, between 84 and 89% of the *A. limnaeus* genome is represented in the current draft genome assembly. Core Eukaryotic Genes Mapping Approach (CEGMA) results indicate that 68.97% (complete) and 95.96% (partial/complete) of 248 highly conserved eukaryotic genes are present in the assembly (Table 3). Benchmarking Universal Single-Copy Orthologs (BUSCO) analysis using 3023 conserved vertebrate genes indicates that 75% of these are completely present in the assembly, 1.6% are duplicated, 12% are fragmented, and 11% are missing (Table 4). This draft assembly *Austrofundulus limnaeus* 1.0 (GenBank accession GCA_001266775.1) was annotated using the NCBI Eukaryotic Genome Annotation Pipeline. A total of 9.3 billion RNA-seq reads were aligned to the *A. limnaeus* genome at an average alignment frequency of 73%. This automated pipeline was able to annotate 26,157 genes and is publicly available on NCBI as the *Austrofundulus limnaeus* Annotation Release 100. The complete feature results of the NCBI Eukaryotic Genome Annotation Pipeline for *A. limnaeus* are shown in Tables 5 and 6.

Using k-mer frequency, Allpaths-LG predicted the *A. limnaeus* genome to have a G + C content of 41.6%, an overall single nucleotide polymorphism rate of 1 in 147 bases, and to be 46% repetitive (Table 1). The total

Table 1 Species comparison of total estimated genomic GC and repeat content

Species	Genome size[a] (gb)	GC%	Repetitive%	References
A. limnaeus	0.974–1.03	41.6	46	This work
Zebrafish	1.41	50.6	52.2	[94]
N. furzeri	1.3–1.9	44.9	45	[40] [30]
Stickleback	0.461	50.5	6.6	[95]
Cod	0.83	50.0	25.4	[96]
Human	3.1	46.1	66–69	NSDC Assembly GCA_000001405.17, [97, 98]

[a]The estimated genome size ranges of *A. limnaeus* and *N. furzeri* are based on flow cytometry and computational methods. For all others, the genome sizes are based on total assembly length

Wagner *et al. BMC Genomics* (2018) 19:155

Page 4 of 21

Table 3 CEGMA analysis report comparing completeness of different teleost genomes

Species	Database	Assembly	Percent complete	Percent partial or complete
Austrofundulus limnaeus	NCBI	GCA_001266775.1	68.97% (171/248)	95.96% (237/248)
Nothobranchius furzeri (FLI)	NCBI	GCA_001465895.2	79.44% (197/248)	96.77% (240/248)
Nothobranchius furzeri (Stanford)	NCBI	GCA_000878545.1	76.61% (190/248)	96.77% (240/248)
Fundulus heteroclitus	NCBI	GCA_000826765.1	79.44% (197/248)	96.77% (240/248)
Gadus morhua	Ensembl	gadMor1	63.71% (158/248)	95.97 (238/248)
Gasterosteus aculeatus	Ensembl	BROAD S1	86.29% (214/248)	97.58 (242/248)
Kryptolebias marmoratus[a]	–	–	83.87% (208/248)	95.16% (236/248)

[a]CEGMA results for *K. marmoratus* are from Kelley et al. [99]

repeat content in the *A. limnaeus* genome is much higher than other teleost species such as *Gasterosteus aculeatus* (stickleback) and *Gadus morhua* (cod), but is very similar to *N. furzeri* and *D. rerio* (Table 1). Repeat-Modeler was able to detect approximately 30% of the assembled genome as repetitive elements (Table 7).

Positive selection in *A. limnaeus* genes associated with mitochondrial function

To identify genes that may support the unique biology of *A. limnaeus*, we utilized a comparative approach to find genes under possible positive selection in the lineage. We collected highly conserved protein coding genes from several teleost species and generated a phylogenetic tree with strong node support (Fig. 2; Additional file 1: Table S1A). *A. limnaeus* is sister to the Family Nothobranchiidae, which includes the African annual killifish genus *Nothobranchius* as well as the non-annual African killifish *A. striatum*. Of the 4152 gene families that passed our filters for PAML analysis, 105 genes were determined to have at least one significantly selected site along the *A. limnaeus* branch (FDR < 0.2, Additional file 1: Table S1B). Several GO terms within the biological process, molecular function, and cellular component categories are significantly enriched among this list of genes (adjusted $P \leq 0.05$, Fig. 3; Additional file 1: Table S1C). To further interrogate these 105 genes, we compared the list to 249 genes previously reported by Valenzano et al. to be under putative

positive selection along the *N. furzeri* branch [30]. Of these 249 genes, eight orthologs were also called by PAML as having at least one site under selection in *A. limnaeus* (Fig. 4a,b). Overall, we found that 24 out of 105 (23%) of the genes under putative positive selection in *A. limnaeus* annotated to nuclear genes associated with mitochondrial biogenesis or activity (Fig. 5).

Differential expression of DII RNAs following anoxia or exit from DII

Among the three embryo groups used in this study (DII normoxia, DII 24 h anoxia, 4 dpd normoxia) we found that 12,049 and 381 genes were shared between the groups at abundance thresholds of Fragments Per Kilobase of transcript per Million mapped reads (FPKM) ≥ 2 and FPKM ≥ 100, respectively (Fig. 6).

Gene expression of DII embryos in anoxia

Following 24 h of anoxia in DII embryos, the vast majority of transcripts do not change in abundance. Of the transcripts expressed that reached our FPKM threshold, 294 transcripts increased in abundance, while 68 transcripts decreased in abundance (false discovery rate, FDR adjusted $P < 0.05$; Fig. 7, Fig. 8A; Additional file 1: Table S1D). Several of the transcripts with the largest increases in FPKM included proteins involved in the heat shock response (Table 8). GO terms for genes that increased in abundance were enriched for localization, metabolism, and the misfolded protein process (adjusted

Table 4 BUSCO analysis report comparing completeness of different teleost genomes

Species	Database	Assembly	BUSCO database	Complete	Duplicated	Fragmented	Missing	n
Austrofundulus limnaeus	NCBI	GCA_001266775.1	vertebrata	75%	1.6%	12%	11%	3023
Nothobranchius furzeri (FLI)	NCBI	GCA_001465895.2	vertebrata	76%	1.3%	13%	9.3%	3023
Nothobranchius furzeri (Stanford)	NCBI	GCA_000878545.1	vertebrata	73%	1.8%	15%	11%	3023
Danio rerio	Ensembl	GRCz10	vertebrata	80%	3.4%	12%	6.1%	3023
Fundulus heteroclitus	NCBI	GCA_000826765.1	vertebrata	80%	1.8%	11%	8.3%	3023
Gadus morhua	Ensembl	gadMor1	vertebrata	69%	1%	17%	13%	3023
Gasterosteus aculeatus	Ensembl	BROAD S1	vertebrata	85%	2.3%	9.70%	4.8%	3023
Kryptolebias marmoratus[a]	–	–	vertebrata	76.5%	1.6%	10.20%	13.3%	3023

[a]*K. marmoratus* BUSCO results were obtained from Kelley et al. [99]

Wagner *et al. BMC Genomics* (2018) 19:155

Page 5 of 21

Table 5 NCBI Eukaryotic Genome Annotation Pipeline feature report for the *A. limnaeus* genome

Feature	Count	Mean length (bp)	Median length (bp)	Min length (bp)	Max length (bp)
Genes	26,157	18,385	8286	71	638,625
All transcripts	38,958	2868	2288	71	88,923
mRNA	35,329	3063	2454	183	88,923
misc_RNA	370	2747	2371	115	13,579
tRNA	441	74	73	71	87
lncRNA	2818	884	676	89	6645
Single-exon transcripts	1638	1516	1291	183	7265
coding transcripts (NM_/XM_)	1638	1516	1291	183	7265
CDSs	35,329	2011	1434	96	87,576
Exons	246,940	264	137	2	17,283
in coding transcripts (NM_/XM_)	239,150	262	136	2	17,283
in non-coding transcripts (NR_/XR_)	10,381	281	140	2	7351
Introns	215,079	2084	353	8	369,543
in coding transcripts (NM_/XM_)	210,044	2037	351	8	369,543
in non-coding transcripts (NR_/XR_)	7596	3392	463	30	180,124

Table 6 Support for gene models using the NCBI Eukaryotic Genome Annotation Pipeline

Feature	Count
Genes and pseudogenes	26,712
protein-coding	23,844
non-coding	2313
pseudogenes	555
genes with variants	6136
mRNAs	35,329
fully-supported	33,945
with > 5% ab initio	552
partial	11,187
with filled gap(s)	10,926
known RefSeq (NM_)	0
model RefSeq (XM_)	35,329
Other RNAs	3629
fully-supported	3188
with > 5% ab initio	0
partial	36
with filled gap(s)	36
known RefSeq (NR_)	0
model RefSeq (XR_)	3188
CDSs	35,368
fully-supported	33,945
with > 5% ab initio	639
partial	9918
with major correction(s)	3568
known RefSeq (NP_)	0
model RefSeq (XP_)	35,329

$P < 0.01$, Fig. 9; Additional file 1: Table S1E). Of the transcripts that significantly decreased in abundance, the top four with the largest decreases in FPKM relative to normoxia are all components of complex I, and all ten are transcripts associated with mitochondria (Table 8). Significantly enriched GO terms for genes that decreased in transcript abundance showed enrichment for localization, metabolism, development, and response to stimulus (adjusted $P < 0.01$, Fig. 9; Additional file 1: Table S1F).
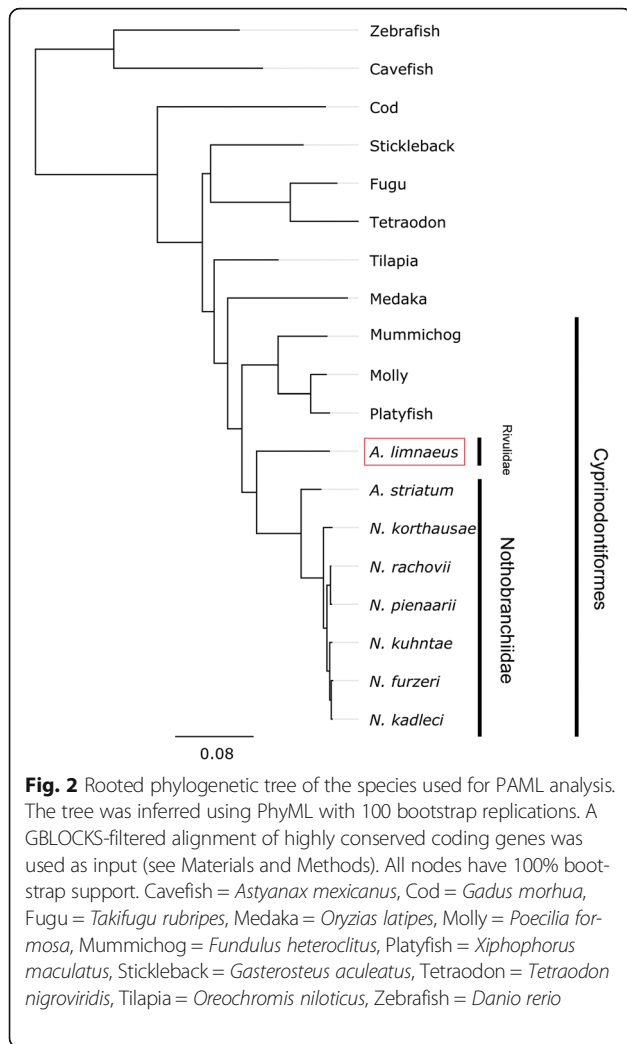
Gene expression following exit of DII

Relative to normoxic DII embryos, we found 7600 genes to change in abundance in 4 dpd embryos (FDR,

Table 7 Identified repeat classes in *A. limnaeus* using RepeatModeler and compared to zebrafish (*D. rerio*)

	A. limnaeus	D. rerio	
Repeat Masker %	27.55	–	
Tandem repeat finder %	3.13	–	
Total % identified[a]	30.68	52.2	
Repeat class/superfamily[a]			Type
SINE %	0.69	2.216	type I transposons
LINE %	3.89	2.58	type I transposons
LTR elements %	0.77	3.314	type I transposons
non-LTR elements	–	2.495	type I transposons
DNA elements %	6.36	38.51	type II transposons
Unclassified	15.22	0.05	
Simple repeats %	0.42	6.44	
Low complexity	0.42	10.68	

[a]Repeat categories are listed as percentages of their respective whole genomes

Wagner *et al. BMC Genomics* (2018) 19:155

Page 6 of 21

Fig. 2 Rooted phylogenetic tree of the species used for PAML analysis. The tree was inferred using PhyML with 100 bootstrap replications. A GBLOCKS-filtered alignment of highly conserved coding genes was used as input (see Materials and Methods). All nodes have 100% boot-strap support. Cavefish = *Astyanax mexicanus*, Cod = *Gadus morhua*, Fugu = *Takifugu rubripes*, Medaka = *Oryzias latipes*, Molly = *Poecilia formosa*, Mummichog = *Fundulus heteroclitus*, Platyfish = *Xiphophorus maculatus*, Stickleback = *Gasterosteus aculeatus*, Tetraodon = *Tetraodon nigroviridis*, Tilapia = *Oreochromis niloticus*, Zebrafish = *Danio rerio*
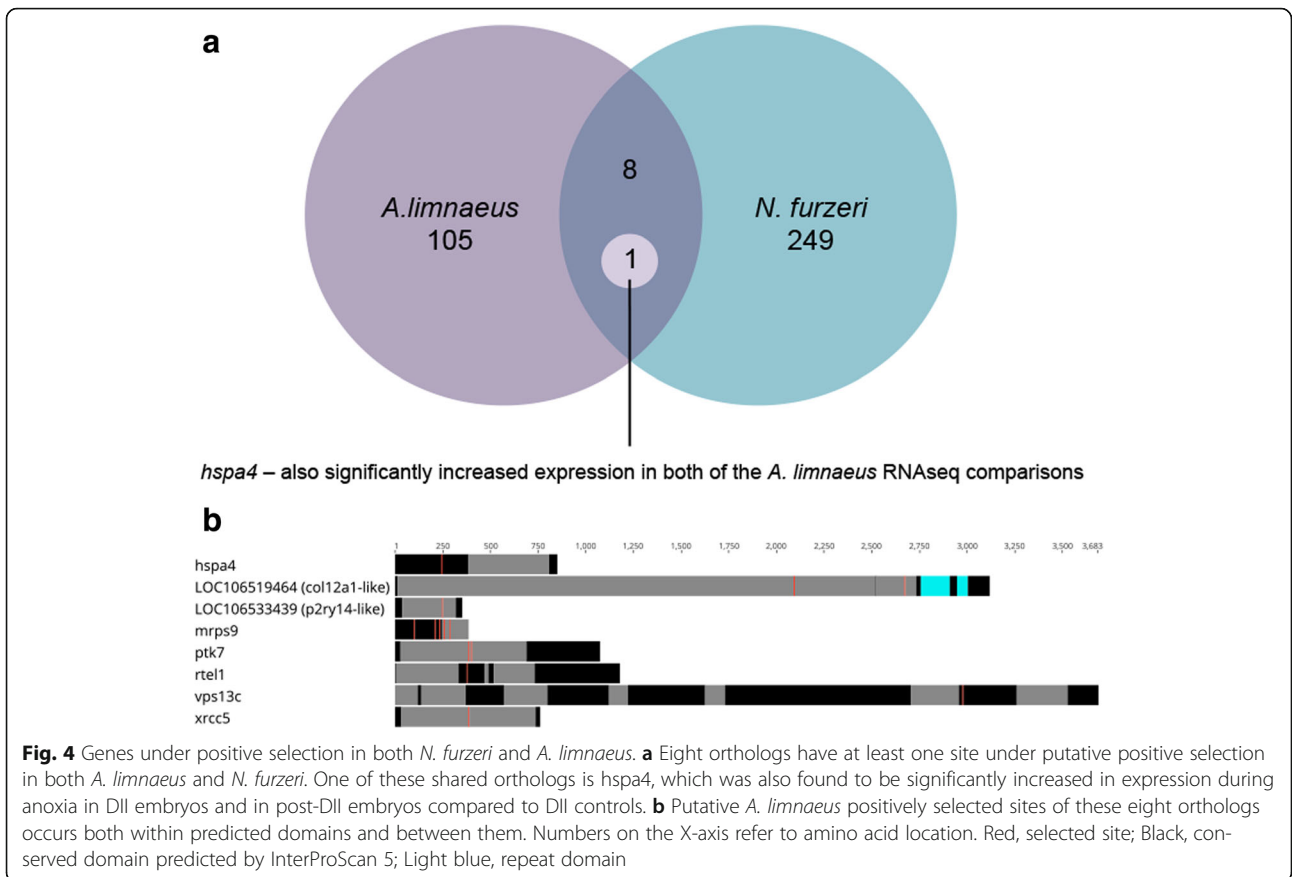
adjusted P < 0.05; Fig. 7; Additional file 1: Table S1G). In contrast to the comparison of transcript changes in anoxia, there is a roughly even split between number of genes that increase (4139) or decrease (3469) in abundance (Fig. 8a). There was very little overlap between the transcripts that are differentially expressed in anoxia and upon exit from diapause II (Fig. 8b). We observed several hemoglobin subunit transcripts to be highly increased in FPKM in 4 dpd embryos, while the top transcripts that decreased were generally more diverse (Table 9). GO enrichment analysis for the post-diapause II (4 dpd) embryo transcripts that were differentially expressed indicated enrichment for terms involved in localization, metabolic processes, cellular processes, and development (adjusted P < 0.01, Fig. 10; Additional file 1: Table S1H, I). Additionally, GO term enrichment for cell cycle was unique to transcripts that increased in abundance, while term enrichment for regulation, signaling, locomotion, and biological adhesion were unique for those that decreased in abundance.

Transcriptional expression of stress response genes

When compared to normoxic DII controls, we observed 101 genes related to heat shock proteins (hsps), accessory heat shock proteins, or related to the general stress response to be significantly differentially expressed in both anoxia and post-DII development (Fig. 11). Although there were not any apparent trends in expression profiles between the two comparisons, a majority of the significantly differentially expressed 70-kDa heat shock protein (hsp70) family transcripts had an inverse expression profile between these comparisons (Additional file 1: Table S1J). The gene hspa4, also a part of the hsp70 family, was also determined to be under positive selection by PAML analysis. In *A. limnaeus*, the residue change in hspa4
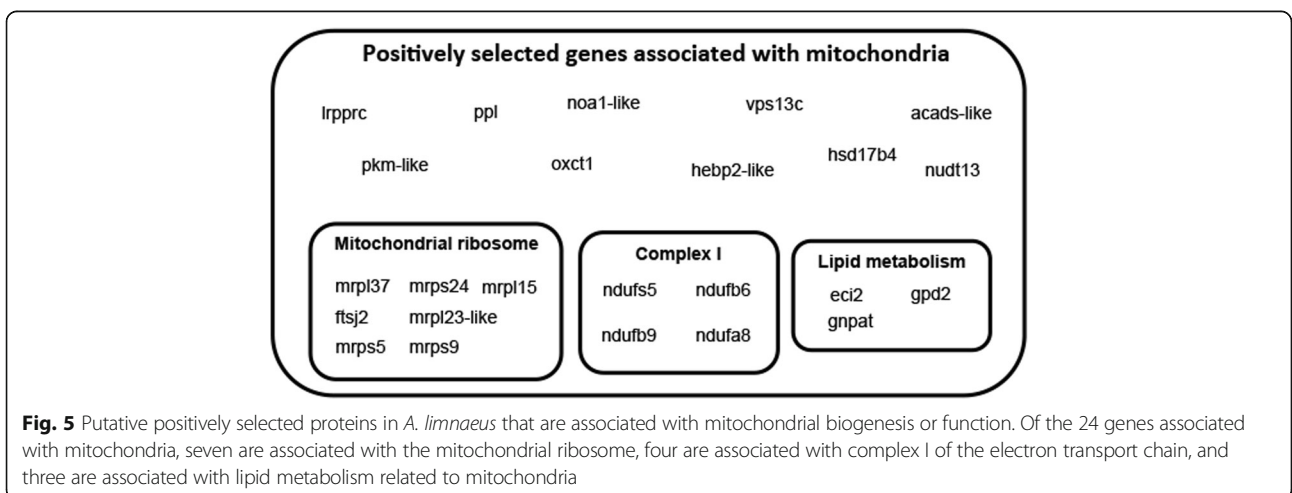

Fig. 3 Significantly enriched GO terms for genes under putative positive selection (adjusted *P*-value ≤0.05). The numbers within the bars indicate the total number of *A. limnaeus* genes associated with the GO term that were determined to be under putative positive selection following PAML analysis. BP, biological process; MF, molecular function; CC, cellular component

Wagner *et al. BMC Genomics* (2018) 19:155

Page 7 of 21

Fig. 4 Genes under positive selection in both *N. furzeri* and *A. limnaeus*. **a** Eight orthologs have at least one site under putative positive selection in both *A. limnaeus* and *N. furzeri*. One of these shared orthologs is hspa4, which was also found to be significantly increased in expression during anoxia in DII embryos and in post-DII embryos compared to DII controls. **b** Putative *A. limnaeus* positively selected sites of these eight orthologs occurs both within predicted domains and between them. Numbers on the X-axis refer to amino acid location. Red, selected site; Black, conserved domain predicted by InterProScan 5; Light blue, repeat domain

appears to be from an ancestral cysteine to a valine, amino acids that are polar and nonpolar, respectively (Fig. 12).

Discussion

Size, structure, and annotation quality of the *A. limnaeus* genome

The *A. limnaeus* nuclear genome has been previously reported to contain 22 haploid chromosomes [38].

However, direct or sequence-based measurements of genome size in this species has not yet been determined. The *A. limnaeus* genome is estimated to be slightly larger than the cod genome, but much smaller than *N. furzeri* and *D. rerio*. We observed the *A. limnaeus* genome to be highly repetitive, and our assembly benefitted heavily from the use of mate-pair libraries for scaffolding. Interestingly, nearly half of the
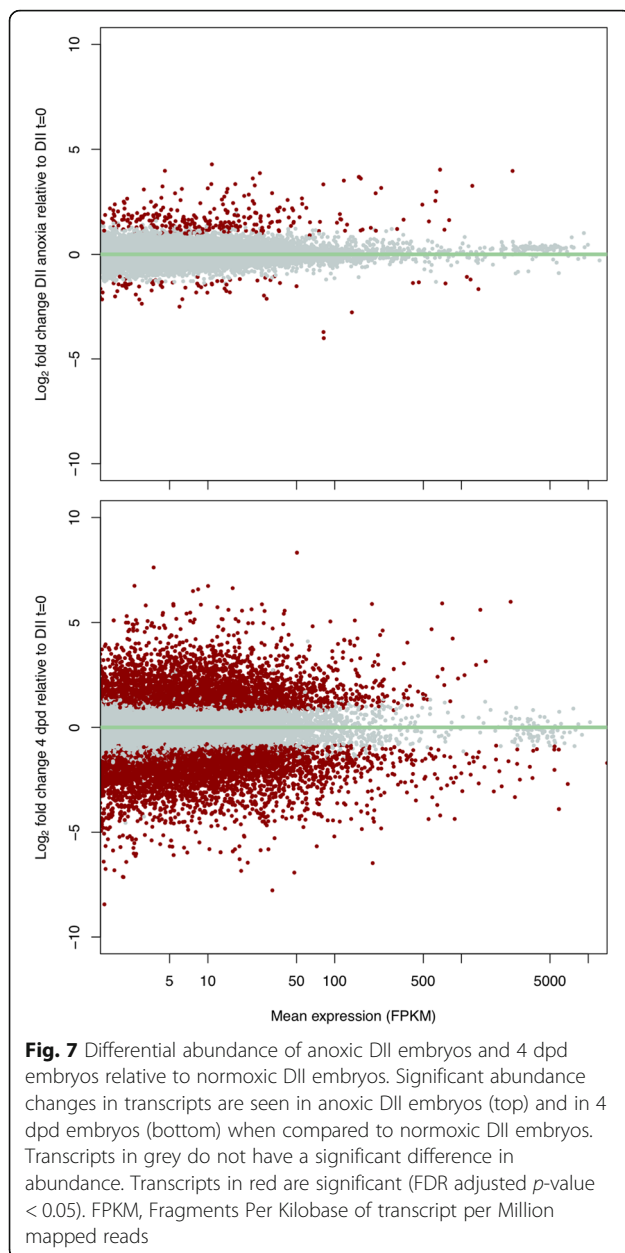

Fig. 5 Putative positively selected proteins in *A. limnaeus* that are associated with mitochondrial biogenesis or function. Of the 24 genes associated with mitochondria, seven are associated with the mitochondrial ribosome, four are associated with complex I of the electron transport chain, and three are associated with lipid metabolism related to mitochondria

Wagner *et al. BMC Genomics* (2018) 19:155

Page 8 of 21

Fig. 6 Overlap in the expression of genes between the three groups examined in this work. Venn diagrams are shown at FPKM thresholds of ≥2 (top) and ≥100 (bottom) to compare the normoxic DII, anoxic DII, and 4 dpd embryo RNA-seq data sets used in this work

repetitive elements in the *A. limnaeus* genome were unable to be classified, a result similar to findings in *Nothobranchius* and another South American annual killifish, *Austrolebias charrua* [39, 40]. Comparing these unclassified repeat elements between annual killifish species may reveal possible conserved mechanisms of genome expansion and evolution in killifishes. Despite the highly repetitive structure of the *A. limnaeus* genome, BUSCO analysis examining 3023 conserved vertebrate genes indicates that the *A. limnaeus* draft genome has completeness and fragmentation similar to the genomes of *N. furzeri* and *K. marmoratus*, two closely related species assembled with similar strategies. Overall, the *A. limnaeus* genome currently contains highly complete gene models, but may benefit from longer reads in the future to patch the extensively repetitive regions occurring between genic sites.

Several mitochondrial related genes may be under positive selection in *A. limnaeus*

Our phylogenetic tree places *A. limnaeus* sister to the Family Nothobranchiidae, and nested within the Order Cyprinodontiformes, which agrees with previous reports [32, 34]. PAML analysis identified 105 genes to have at least one significantly selected site along the *A. limnaeus* branch. Several GO terms of relevance to annual killifish biology are significantly enriched among this list of genes, including stress tolerance and oxidation-reduction activity [21, 41]. Reichwald et al. [31] found seven genes under positive selection along the *N. furzeri* branch and one along the *N. pienaari* branch, but we did not find the same orthologs for these *Nothobranchius* species to also be under selection in the *A. limnaeus* branch using our analysis. When compared to the list of genes under putative positive selection in *N.*

Wagner *et al. BMC Genomics* (2018) 19:155

Page 9 of 21

Fig. 7 Differential abundance of anoxic DII embryos and 4 dpd embryos relative to normoxic DII embryos. Significant abundance changes in transcripts are seen in anoxic DII embryos (top) and in 4 dpd embryos (bottom) when compared to normoxic DII embryos. Transcripts in grey do not have a significant difference in abundance. Transcripts in red are significant (FDR adjusted *p*-value < 0.05). FPKM, Fragments Per Kilobase of transcript per Million mapped reads

furzeri by Valenzano et al. [30], the eight shared positively selected genes had selected sites both inside and outside of predicted protein domain regions. This suggests that selection may be operating at the level of domain function as well as the tertiary structure of the proteins, and while some genes may be positively selected in both lineages, there may also be extensive differences in which genes are under selection in other annual killifish lineages.

In a recent report by Sahm et al. [42], multiple nuclear genes involved with mitochondrial biogenesis or activity were also found to be under putative positive selection along several *Nothobranchius* branches associated with

shortened lifespan. Our results suggest that only NADH:Ubiquinone Oxidoreductase Subunit S5 (ndufs5) is under putative positive selection along both the *A. limnaeus* branch and the *Nothobranchius* branch containing the last common ancestor of *N. pienaari* and *N. rachovii* previously reported by Sahm et al. [42]. However, the annual killifish phenotype is a complex mix of several phenotypes and we note that our strain of *A. limnaeus* does not exhibit the shortened lifespan of several *Nothobranchius* species, nor do *Nothobranchius* species appear to have the extreme anoxia tolerance of *A. limnaeus* (Polačik and Podrabsky, unpublished). These results raise the possibility that the proteins under positive selection in *A. limnaeus* or in *Nothobranchius* species may be involved in different aspects of annual killifish biology, such as with stress tolerance in *A. limnaeus*, and aging in several *Nothobranchius* species.

Interestingly, four of the genes under putative positive selection include NADH:Ubiquinone Oxidoreductase accessory subunits that are a part of complex I, an enzyme complex located in the inner mitochondrial membrane that is also the first enzyme of the mitochondrial electron transport chain [43]. Recent evidence has suggested that several complex I subunits encoded by the *A. limnaeus* mitochondrial genome (mtgenome) have apparent insertions or deletions at the N-terminus when compared to multiple other teleost species within the Order Cyprinodontiformes [44]. One of these mtgenome-encoded complex I subunits, ND5 contains a unique 11 amino acid insertion in the N-terminus and is thought to interact directly with one of the complex I accessory subunits we have identified to be under putative positive selection, ndufb6 [45]. Importantly, complex I is thought to be a primary source of reactive oxygen species (ROS) generation, and control of ROS production is likely essential for surviving anoxia [46–48]. Because mitochondria perform essential energy-generating processes, it is likely that nuclear genome evolution will favor mutations that can accommodate changes in mtgenome sequence [49]. However, it is unclear if this is a case of mitonuclear co-evolution to promote the unique stress-tolerant phenotype of *A. limnaeus*, or compensation of nuclear genes to prevent complex I dysfunction. Further investigations into the role of the complex I subunits and possible roles in ROS production or suppression may yield important insight into the evolution of dormancy and anoxia tolerance in this lineage.

DII embryos have a transcriptional response to anoxia treatment

We were interested in gene expression changes that may facilitate extreme anoxia tolerance in *A. limnaeus* DII embryos, Therefore, we used RNAseq to compare transcript abundance in DII embryos after 24 h of anoxia

Wagner *et al. BMC Genomics* (2018) 19:155

Page 10 of 21

Fig. 8 Summary of *A. limnaeus* embryo differential transcript abundance analysis. **a** Transcripts that change significantly in abundance relative to normoxic DII embryos (FDR adjusted *p*-value < 0.05). **b** The number of significantly differentially expressed transcripts that overlap among possible comparisons
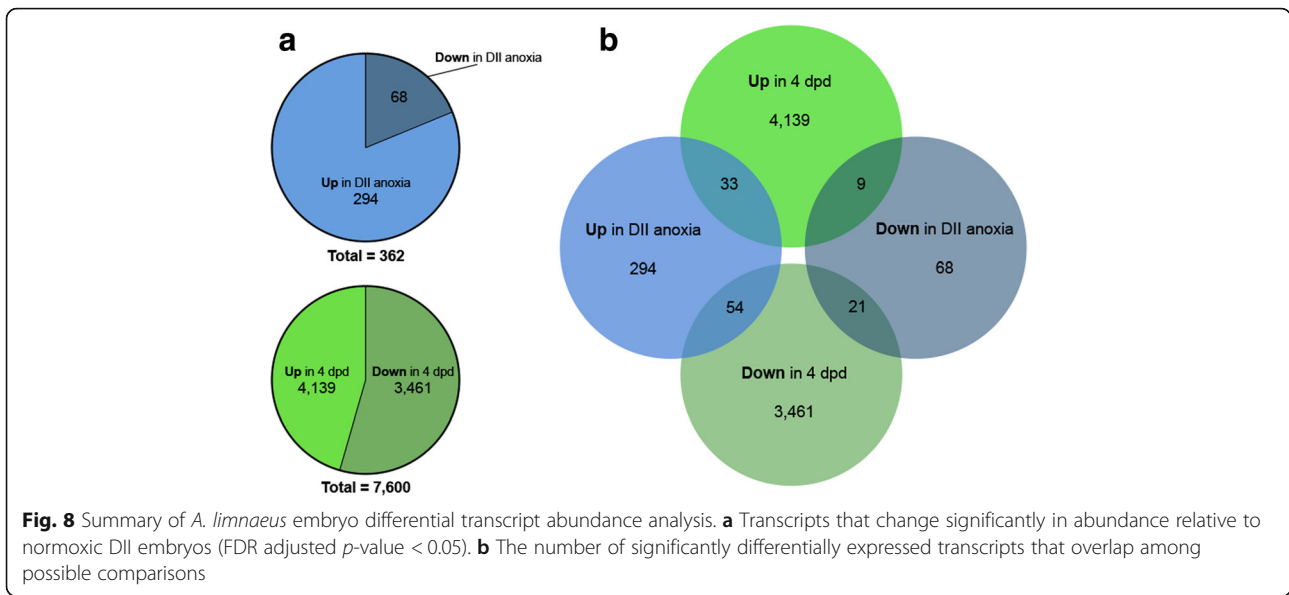
relative to normoxic DII embryos. Following anoxia treatment, we observed that the majority of transcripts do not have a significant change in abundance. This observation suggests an overall stabilization of the transcriptome during exposure to anoxia consistent with

available data and theory [50–52]. Unexpectedly, 294 transcripts increased in abundance, supporting active regulation of a small portion of the transcriptome through either increased synthesis or possibly differential stabilization. Not surprisingly, many of the genes with

Table 8 Top 10 genes in anoxic DII embryos with greatest transcript abundance changes relative to normoxia

	Gene symbol	Gene type	Description	P-value[a]	ΔFPKM[b]
Up	LOC106513602	protein coding	heat shock protein 30-like	2.12E-28	4786
	pck1	protein coding	phosphoenolpyruvate carboxykinase 1	6.00E-28	2099
	LOC106513603	protein coding	heat shock protein 30-like	3.23E-22	1332
	LOC106520367	protein coding	heat shock cognate 71 kDa protein-like	1.06E-30	1028
	LOC106533043	protein coding	heat shock protein HSP 90-alpha-like	4.86E-22	926
	sqstm1	protein coding	sequestosome 1	9.59E-07	873
	LOC106523747	protein coding	apolipoprotein A-I-like	9.82E-20	697
	LOC106534642	pseudo	ubiquitin-like	3.83E-02	608
	LOC106535465	pseudo	ubiquitin-like	3.50E-06	585
	LOC106531886	protein coding	wiskott-Aldrich syndrome protein family member 2-like	1.43E-02	445
Down	ND6	protein coding	Mitochondrially encoded NADH:Ubiquinone Oxidoreductase Core Subunit 6	1.43E-04	-1595
	ND2	protein coding	Mitochondrially encoded NADH:Ubiquinone Oxidoreductase Core Subunit 2	6.28E-05	− 969
	ND1	protein coding	Mitochondrially encoded NADH:Ubiquinone Oxidoreductase Core Subunit 1	1.10E-02	− 823
	ND5	protein coding	Mitochondrially encoded NADH:Ubiquinone Oxidoreductase Core Subunit 5	2.47E-02	−775
	16S	rRNA	Mitochondrially encoded 16S ribosomal RNA	8.74E-03	− 441
	LOC106511533	protein coding	NADH-ubiquinone oxidoreductase chain 5-like	4.44E-02	− 429
	Pseudo16S	pseudo	Mitochondrially encoded 16S rRNA pseudogene	1.38E-19	− 219
	tRNALeu2–1	tRNA	Mitochondrial tRNA Leu2 copy 1	2.73E-41	−153
	tRNALeu2–2	tRNA	Mitochondrial tRNA Leu2 copy 2	1.10E-34	−149
	txnip	protein coding	thioredoxin interacting protein	4.61E-08	−51

[a]FDR adjusted P-value
[b]Change in mean FPKM values of DII embryos in anoxia relative to DII t = 0
FPKM, Fragments per kilobase of transcript per million mapped reads

Wagner *et al. BMC Genomics* (2018) 19:155

Page 11 of 21

Fig. 9 Significantly enriched GO terms based on differential abundance analysis of anoxic and normoxic DII embryos. Only terms with an adjusted P of < 0.01 are shown. Numbers in the bars indicate the total number of transcripts that change in abundance associated with the respective GO term
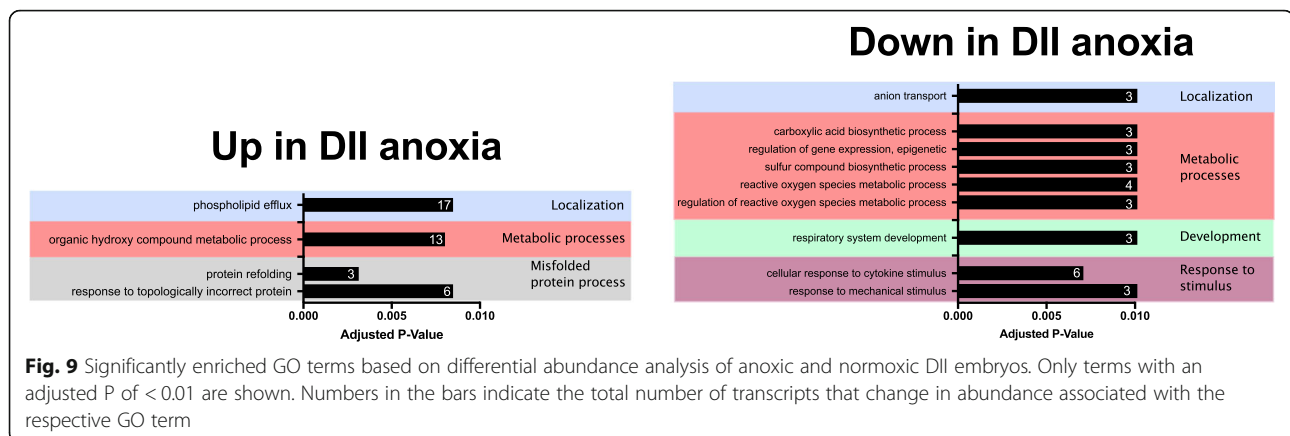
the largest increases in abundance are associated with the cellular stress response. Of note, two hsp30-like transcripts ranked as numbers 1 and 3 in transcripts that increased in abundance. Others have reported on the importance of hsp30 proteins in the heat shock response of desert fishes, although their functional importance has not been experimentally explored [53, 54]. Relatively fewer transcripts decreased in abundance, and many of these genes are indicated by GO term enrichment analysis to be associated with metabolism. This suggests a

trend towards further decreasing metabolic processes during anoxia even though the embryos are already in a highly metabolically depressed state.

Interestingly, the majority of transcripts in anoxic DII embryos that had the greatest decreases in FPKM relative to normoxic controls are associated with the mitochondrial transcriptome. Previous work has suggested that regulation of mtgenome-encoded ND5 through differential stabilization of *ND5* mRNA, rather than mitochondrial DNA copy number, may be the rate-limiting

Table 9 Top 10 genes in 4 dpd embryos with greatest transcript abundance changes relative to normoxic diapause II embryos

	Gene symbol	Gene type	Description	P-value[a]	ΔFPKM[b]
Up	LOC106528963	protein coding	hemoglobin embryonic subunit alpha	3.15E-38	4755
	LOC106528894	protein coding	hemoglobin subunit beta-like	4.10E-28	2717
	LOC106523751	ncRNA	uncharacterized	3.32E-26	2492
	LOC106512448	pseudo	fatty acid-binding protein, brain pseudogene	1.96E-08	2045
	LOC106525147	protein coding	hemoglobin subunit alpha-1-like	5.69E-45	1539
	LOC106522944	protein coding	fatty acid-binding protein, brain	1.31E-15	1483
	LOC106528904	protein coding	hemoglobin embryonic subunit alpha-like	1.01E-25	1370
	Pseudo16S	pseudo	Mitochondrially encoded 16S rRNA pseudogene	9.28E-05	1281
	LOC106525143	protein coding	hemoglobin subunit beta-like	8.06E-41	1079
	LOC106511047	protein coding	prothymosin alpha-B-like	9.16E-48	1062
Down	LOC106535866	protein coding	heat shock cognate 70 kDa protein	2.28E-16	−14,958
	LOC106517545	protein coding	lipocalin-like	1.35E-25	−10,327
	LOC106513764	ncRNA	uncharacterized	6.84E-06	−10,299
	ahsg	protein coding	alpha 2-HS glycoprotein	4.25E-11	− 6618
	LOC106524240	protein coding	galactose-specific lectin nattectin-like	1.47E-05	− 5070
	ccng1	protein coding	cyclin G1	6.56E-25	− 4354
	LOC106529138	protein coding	elongation factor 1-alpha-like	2.18E-04	− 4141
	LOC106518780	protein coding	keratin, type I cytoskeletal 19-like	1.06E-19	− 4062
	LOC106526789	protein coding	ferritin, middle subunit	3.16E-11	− 4003
	ubb	protein coding	ubiquitin B	8.06E-03	− 3830

[a]FDR adjusted P-value
[b]Change in mean FPKM values of DII embryos in anoxia relative to DII t = 0
FPKM, Fragments per kilobase of transcript per million mapped reads

Wagner *et al. BMC Genomics* (2018) 19:155

Page 12 of 21

Fig. 10 Significantly enriched GO terms based on differential abundance analysis of 4 dpd and normoxic DII embryos. Only terms with an adjusted P of < 0.01 are shown. Numbers in or near the bars indicate the total number of differentially expressed *A. limnaeus* genes associated with the respective GO term
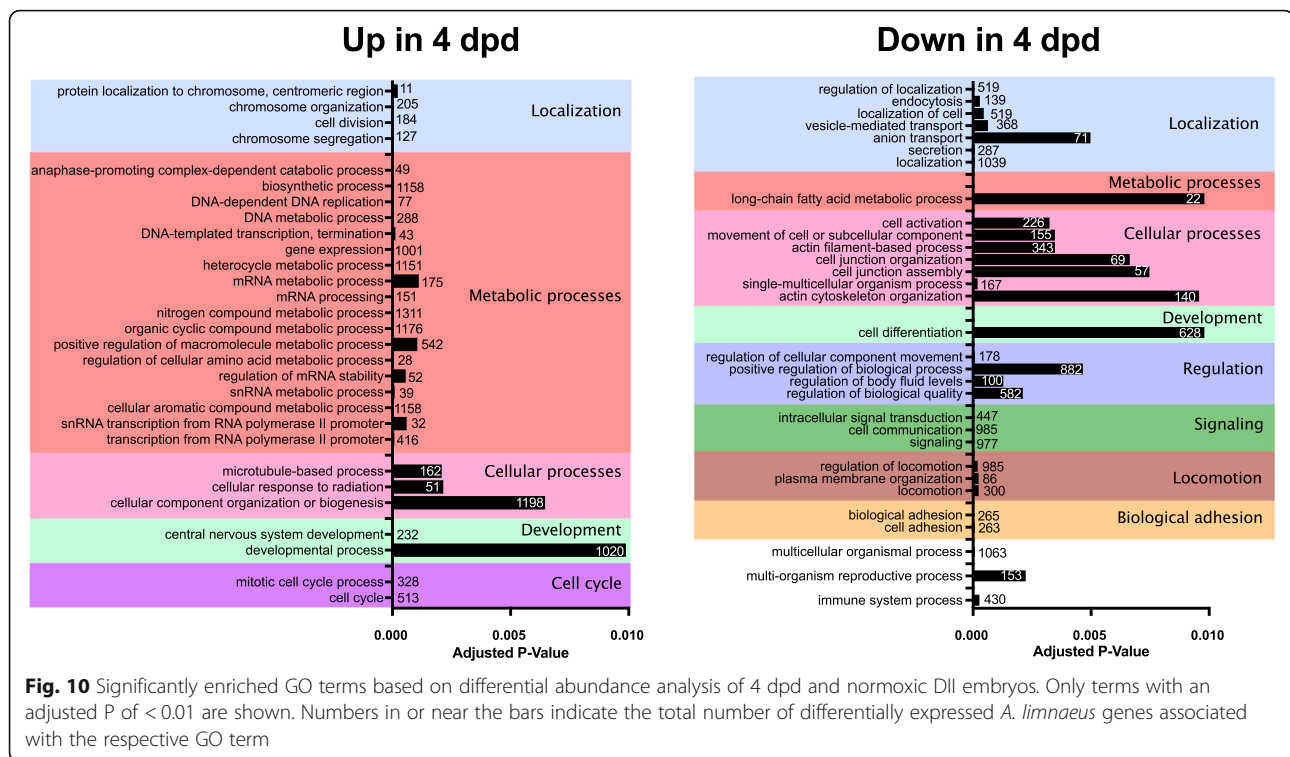
step in the control of cellular respiration [44, 55–58]. While we did observe a significant depression of *ND5* transcripts in anoxic DII embryos, we also found significantly lower abundance of *ND1*, *ND2*, and *ND6* transcripts as well, which indicates that reduced respiration in *A. limnaeus* may be controlled through a coordinated reduction of multiple complex I subunit transcripts rather than just *ND5*. Transcript levels of 16S rRNA decrease during anoxia in *A. limnaeus*, which could lead to a reduction in capacity for mitochondrial protein synthesis. In contrast, transcript abundance for several mitochondrial genes increases in the anoxic turtle brain, suggesting that their mitochondria actually respond by increasing transcription [50]. This divergence in the transcriptome implies different mitochondrial responses to long-term anoxia between turtles and *A. limnaeus* embryos. We also found seven nuclear-encoded proteins with residues under putative positive selection that are involved with mitochondrial translation. However, it is unclear if these proteins have novel functional significance, or if they represent nuclear compensation for rapidly evolving mitochondrial rRNAs following the unique and potentially isolating population dynamics of *A. limnaeus* [59].

Transcriptional response to diapause termination
While previous work has examined transcriptional changes that may be essential for entrance into DII in annual killifish [31], it is currently unclear how DII embryos

may reactivate metabolism and development through changes in RNA expression. The transcript we observed with the greatest decrease in abundance in post-diapause II embryos is a heat shock cognate 70 (*hsc70*) protein with a mean change of − 14,958 FPKM. High abundance of this transcript in diapausing embryos could initially be interpreted to play a role in the increased tolerance to environmental stress observed in these embryos. However, DII and 4 dpd embryos have a similar tolerance of anoxia, with 4 dpd embryos possibly having even higher tolerance, which would suggest a different role for this transcript if the high abundance is translated to high levels of proteins [11]. Interestingly, previous work has shown that hsc70 overexpression promotes degradation of ion channels as they are trafficked through the cell [60]. DII embryos are characterized by an exceptionally low ion permeability that decreases steadily during post-DII development [10], and therefore reduced hsc70 expression may promote increased routing of ion channels to cell membrane surfaces. This would be a unique function for hsc70 in fish embryos that has not yet been described or explored.

Another gene of interest that decreases significantly during post-diapause II development is cyclin G1. This cyclin is known to interact with p53 and is associated with cell cycle arrest at a number of different cell cycle checkpoints [61, 62]. Further exploration of the functional significance of this transcript and its signaling networks may lead to the key players that regulate exit from the cell cycle during diapause in this species.
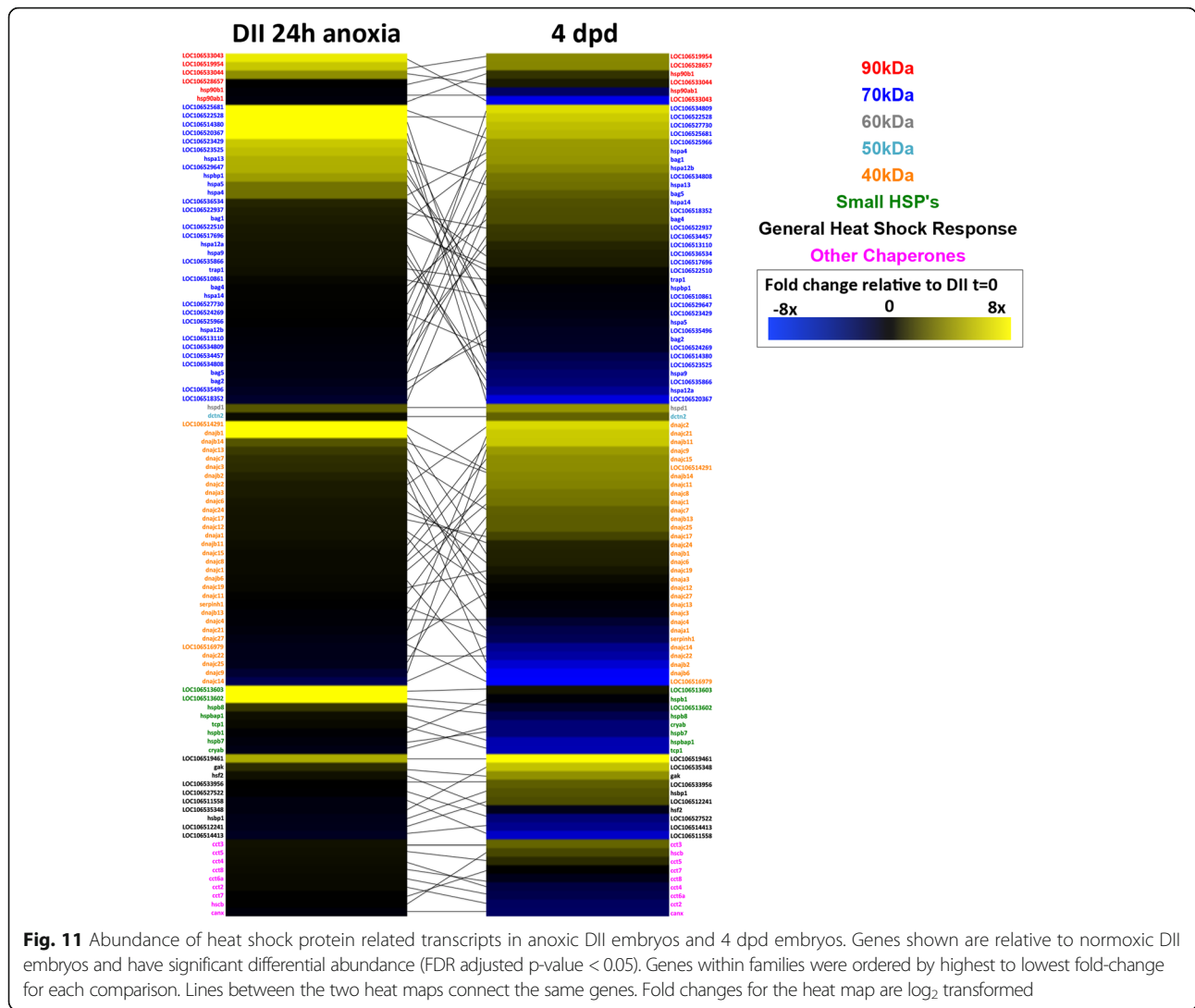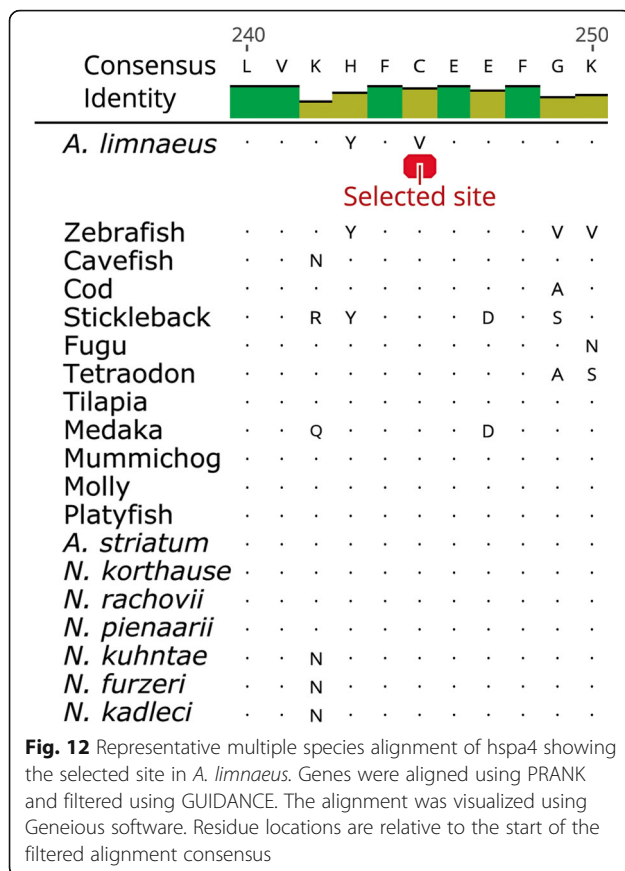
Wagner *et al. BMC Genomics* (2018) 19:155

Page 13 of 21

Fig. 11 Abundance of heat shock protein related transcripts in anoxic DII embryos and 4 dpd embryos. Genes shown are relative to normoxic DII embryos and have significant differential abundance (FDR adjusted p-value < 0.05). Genes within families were ordered by highest to lowest fold-change for each comparison. Lines between the two heat maps connect the same genes. Fold changes for the heat map are log$_2$ transformed

Importantly, most of the transcripts that change drastically during PDII development very likely have little to do with the regulation of diapause, but rather are due to the resumption of active development and the associated changes in tissue differentiation and morphogenesis. For example, several hemoglobin transcripts are among the top ten genes with the greatest increase in abundance compared to diapause II embryos. This increase in abundance coincides with the appearance of red blood cells in the embryos and likely supports their transition to aerobic metabolism as they continue development [7, 22]. A more thorough and mechanistic analysis of pre- and post-diapause expression patterns will be required to identify putative regulators of metabolic dormancy.

Heat shock proteins in annual killifish anoxia tolerance, development, and evolution

Our two RNA-seq comparisons provided a unique opportunity to study genes that may have roles in either stress tolerance or embryonic development, and in some cases, both. Between these two RNA-seq analysis comparisons (DII 24 h anoxia or 4 dpd embryos relative to DII normoxia), we found 101 genes related to hsps, accessory heat shock proteins, or related to the general stress response, to be differentially expressed in both comparisons. Hsps are a conserved group of molecular chaperones that function to facilitate proper folding of newly translated or misfolded proteins during normal and stressed states, but also can have several other functions related to cell cycle, homeostasis, signaling, and apoptosis [63–65]. We observed differential expression of several hsps from the 90, 70, 60, 50, 40, and small kDa classes in both comparisons, and in the anoxia-treated DII embryos we also found a significant GO term enrichment for genes involved in protein refolding and response to topologically incorrect proteins. Heat shock proteins from the 30 kDa, 70 kDa, and 90 kDa families were represented in the list of top 10 transcripts

Wagner et al. BMC Genomics (2018) 19:155

Page 14 of 21

Fig. 12 Representative multiple species alignment of hspa4 showing the selected site in *A. limnaeus*. Genes were aligned using PRANK and filtered using GUIDANCE. The alignment was visualized using Geneious software. Residue locations are relative to the start of the filtered alignment consensus

with the greatest increase in abundance in response to anoxia in diapausing embryos and are likely a direct response to stress. However, we also observed a diversity of hsp transcripts within the 70 kDa and 40 kDa families that increased in abundance during post-diapause II development. Notably, 20 out of 35 hsp70 family transcripts had an inverse abundance profile when the two groups were compared, suggesting stage-specific roles in development that may be independent of stress tolerance. Thus, *A. limnaeus* may be a powerful model for teasing apart the role of hsps in normal development and stress tolerance, both of which likely contribute in major ways to buffering and canalization during vertebrate development.

One of the molecular chaperones that increased in expression for both comparisons is also under putative positive selection in *A. limnaeus* and *N. furzeri* [30]. This gene, hspa4, is a molecular chaperone from the well-studied hsp70 family, and although it was initially thought to be interchangeable with hsc70, it has been previously shown to have separate cellular functions [60]. In hsp70 family proteins, key replacements of cysteine residues with other amino acids has been reported to reduce redox sensitivity and alter responses to oxidative stress (Miyata et al. 2012). Interestingly, the

presence of an inducible hsp70 isoform that is constitutively expressed during *A. limnaeus* early embryonic development and diapause has been previously reported [66]. We found that *hspa4* transcript abundance increased by 26 FPKM (~ 2.5-fold) in anoxic DII embryos. An increase in hsp70 following anoxia has also been reported in the brains of freshwater turtles, but not the brine shrimp *Artemia franciscana,* and thus may be a conserved response in vertebrates [57, 67]. We also found a significant increase (37 FPKM, ~ 3-fold) in abundance of *hspa4* transcripts in post-DII (4 dpd) relative to normoxic DII embryos. Importantly, expression of inducible hsp70 is usually not present in teleost embryos during non-stressful conditions [68–70]. It is possible that unstressed 4 dpd embryos increase expression of *hspa4* during normal development to provide a rapid response to environmental insults, thus suggesting a unique survival strategy among developing aquatic embryos. Taken together, these data indicate that *hspa4* has both physiological and evolutionary importance for stress tolerance, development, and evolution in *A. limnaeus* biology and is an interesting gene for future studies.

Conclusions

Our release of the *A. limnaeus* genome is the first publicly available South American annual killifish genome and complements recent genome publications of the African annual killifish *Nothobranchius furzeri* by two independent research groups [30, 31]. Despite the high repeat content of the *A. limnaeus* genome, the combination of a merged de novo assembly approach and a vast amount of RNA-seq data has allowed us to generate a draft *A. limnaeus* genome with high-confidence gene annotations, on par with other teleost assemblies. This genome assembly is a critical tool for exploration of annual killifishes at the molecular and genetic levels, and will likely significantly accelerate advances in our understanding of this unique group of vertebrates.

Methods

Genome size estimation by flow cytometry

Zebrafish and chicken blood were generously provided by Dr. Kim Brown (Portland State University) and Chrissie Zaerpoor (Kookoolan Farms, Yamhill, OR), respectively. Whole blood from zebrafish ($n = 2$), chicken ($n = 1$), or *A. limnaeus* ($n = 3$) was homogenized in 1 ml of Galbraith buffer (30 mM sodium citrate, 45 mM MgCl$_2$, 20 mM MOPS, 0.1% Triton-X 100, 1 mg ml^{-1} RNAse A, pH 7.2) on ice using a Sorvall Omni-mixer (speed setting 2) and a loose-fitting Teflon pestle for about 20 strokes. Three technical replicates of the chicken blood were analyzed. Homogenates were filtered through a 35 μm mesh screen by centrifugation at 100 x *g* for

Wagner *et al. BMC Genomics* (2018) 19:155

Page 15 of 21

1 min at 4 °C. Dissociated nuclei were stained in 1 mg ml^{-1} propidium iodide for 30 min at room temperature and fluorescence intensity were measured using the BD Accuri C6 flow cytometer at a flow rate of 14 μl min^{-1} for 100,000 counts (BD Biosciences, San Jose, CA). Counts were gated manually to remove noise from cellular debris. Fluorescence peaks were identified and analyzed with the included BD CSampler Software. The genome size of *A. limnaeus* was inferred from linear regression of zebrafish and chicken nuclei fluorescence relative to assembled genome lengths for those two species, including all gaps (Ensembl release 77).

Total genomic DNA extraction of adult tissue
DNA extraction of adult tissues
Adult *A. limnaeus* fish used for sequencing and for spawning were cared for as previously described by Podrabsky (1999) and in accordance with an approved Portland State University Institutional Animal Care and Use Committee protocol (PSU protocol #33). The tissue used for single-individual Illumina sequencing was derived from an adult *A. limnaeus* male (3 months post-hatch, 3.7 g wet mass). The fish was euthanized by immersion in an ice bath for approximately five minutes until fully unresponsive to stimuli followed by cervical transection. Liver, white muscle (skin and scales removed), and brain tissue were removed and transferred to DNA extraction buffer (10 mM Tris, 100 mM EDTA, 0.5% SDS, 200 μg ml^{-1} Proteinase K (Thermo Scientific #EO0491), pH 8.0) at a ratio of 1 mg tissue per 10 μl buffer. Tissues were gently homogenized using a Teflon pestle in 1.5 ml microcentrifuge tubes and incubated for 3 h at 50 °C with agitation every 20–30 min. DNA was extracted by briefly vortexing the homogenates with 1 vol phenol (equilibrated with 10 mM Tris-HCl pH 8.0, 1 mM EDTA) followed by centrifugation at 5000 x *g* for 10 min at 4 °C. The aqueous phases were collected using a wide-bore pipette and extracted with phenol again as described above. Following the second phenol extraction, the aqueous phase containing the DNA was extracted a third time by gentle mixing with 1 volume of chloroform:phenol (1:1) followed by centrifugation at 5000 x *g* for 10 min at 4 °C. The aqueous phase was collected and the DNA precipitated by the addition of NaCl (final concentration of 200 μM) and 2 volumes of 100% EtOH followed by gentle mixing via tube inversion. DNA was pelleted by centrifugation at 16,000 x *g* for 10 min at 4 °C. The DNA pellet was washed twice with 1 ml 70% EtOH. After each wash, the DNA was pelleted by centrifugation at 16,000 x *g* for 5 min at 4 °C. The air-dried (5–10 min at room temperature) DNA pellet was resuspended in 500 μl of RNAse buffer (10 mM Tris, 5 mM EDTA) with 100 μg ml^{-1} DNAse-free RNAse A (Thermo Scientific #EN0531) and incubated at

37 °C for 45 min with occasional tube inversion. The samples were extracted twice more as described above with chloroform:phenol (1:1) followed by precipitation using 0.1 vol of 3 M sodium acetate (pH 5.2), and 2 vol of 100% EtOH. DNA was pelleted by centrifugation at 16,000 x *g* for 10 min at 4 °C and the pellet was washed twice with 1 ml 70% EtOH as described above. The DNA pellets were dried briefly at room temperature and resuspended in 100 μl of buffer EB (10 mM Tris-Cl pH 8.5, Qiagen #19086) at 37 °C with occasional agitation until pellets dissolved completely.

The tissue for mixed-individual Illumina sequencing was collected from three adult male fish. Fish were euthanized as described above and whole brains were extracted. The three brain tissues were extracted using the Qiagen DNeasy Blood and Tissue Kit (Qiagen #69504) according to the manufacturer's instructions.

DNA quantification and quality assessment
DNA purity was determined by observation of A_{260}/A_{280} ratios between 1.8–1.9 using an Infinite M200 Pro plate reader equipped with a NanoQuant plate (Tecan, San Jose, CA, USA), 2 μl of sample, and default software settings (i-control software, Tecan). DNA concentration was determined by using the Quant-iT dsDNA Assay Kit, broad range (Thermo Fisher Scientific #Q33130) according to manufacturer's instructions. DNA integrity was confirmed by observation of high-molecular weight DNA above 20 kb following electrophoresis of 1 μg of total DNA on a 1% agarose gel.

Sequencing and read quality control
Illumina sequencing
DNA sequencing libraries were prepared and sequenced at the University of Oregon High Throughput DNA sequencing and Genomics facility. Purified DNA was sonicated to an average size of 170 bp and was prepared for sequencing using the Nextera library prep kit (Illumina). Larger fragments were sonicated into size ranges of 2 kb – 3 kb, 5 kb – 8 kb, and 10 kb – 15 kb. These large fragments were size-selected by gel electrophoresis and were used for mate-pair libraries (Additional file 2: Table S2A). Fragment and mate-pair libraries from the single *A. limnaeus* male were sequenced on the Illumina Hi-Seq 2500 platform with 101 bp paired-end reads. Mate-pair libraries from the mixed individuals were sequenced on the Illumina Hi-Seq 2000 platform with 101 bp paired-end reads.

Read quality control
Adapters were removed from Illumina reads using Trimmomatic v0.33 [71] in palindrome mode and using the included Illumina adapter list (seed mismatches = 2, palindrome clip threshold = 30, simple clip threshold = 7, minimum adapter length = 1, keep both reads = true).

Wagner *et al. BMC Genomics* (2018) 19:155

Page 16 of 21

Error-correction was performed using the Allpaths error correction module [36]. For scaffolding, mate-pair libraries were further trimmed to 37 bp in length to reduce instances of chimeric reads and remaining reads with quality scores >Q10 across the entire read were used.

Genome assembly strategy

A summary of the assembly and annotation strategy used for the *A. limnaeus* genome is shown in Fig. 13. Adapter-free reads were de novo assembled using two algorithm strategies. The library types and insert sizes used for genome assembly are shown in Additional file 2: Table S2A. First, the untrimmed reads were assembled using the Allpaths-LG pipeline version r44837, which is based on a modified de Brujin graphing algorithm [36]. A total of 707,851,166 fragment library and 678,076,430 jumping library adapter-free reads were used as input

into Allpaths-LG. As suggested by the Allpaths-LG manual, reads that failed to pass the Illumina purity filter were retained in the read pool for de novo assembly. In a separate assembly, the fragment reads were error corrected using Allpaths-LG and de novo assembled using JR-assembler, an assembler that is based on read overlap to extend contigs [72]. Prior to assembly with JR-assembler, reads were trimmed to 90 bp and filtered using the included mdust algorithm. Contigs were ordered into scaffolds within the individual assemblies by using SSPACE Basic 3.0 using the mate-pair libraries listed in Additional file 2: Table S2A and settings that required at least three connections with 70% identity to scaffold two contigs ($-k = 3$, $-a = 0.7$) [73]. The resulting scaffolds were then merged between Allpaths-LG and JR-assembler to provide the best representation of unique scaffolds from both assemblies. L_RNA_Scaffolder software
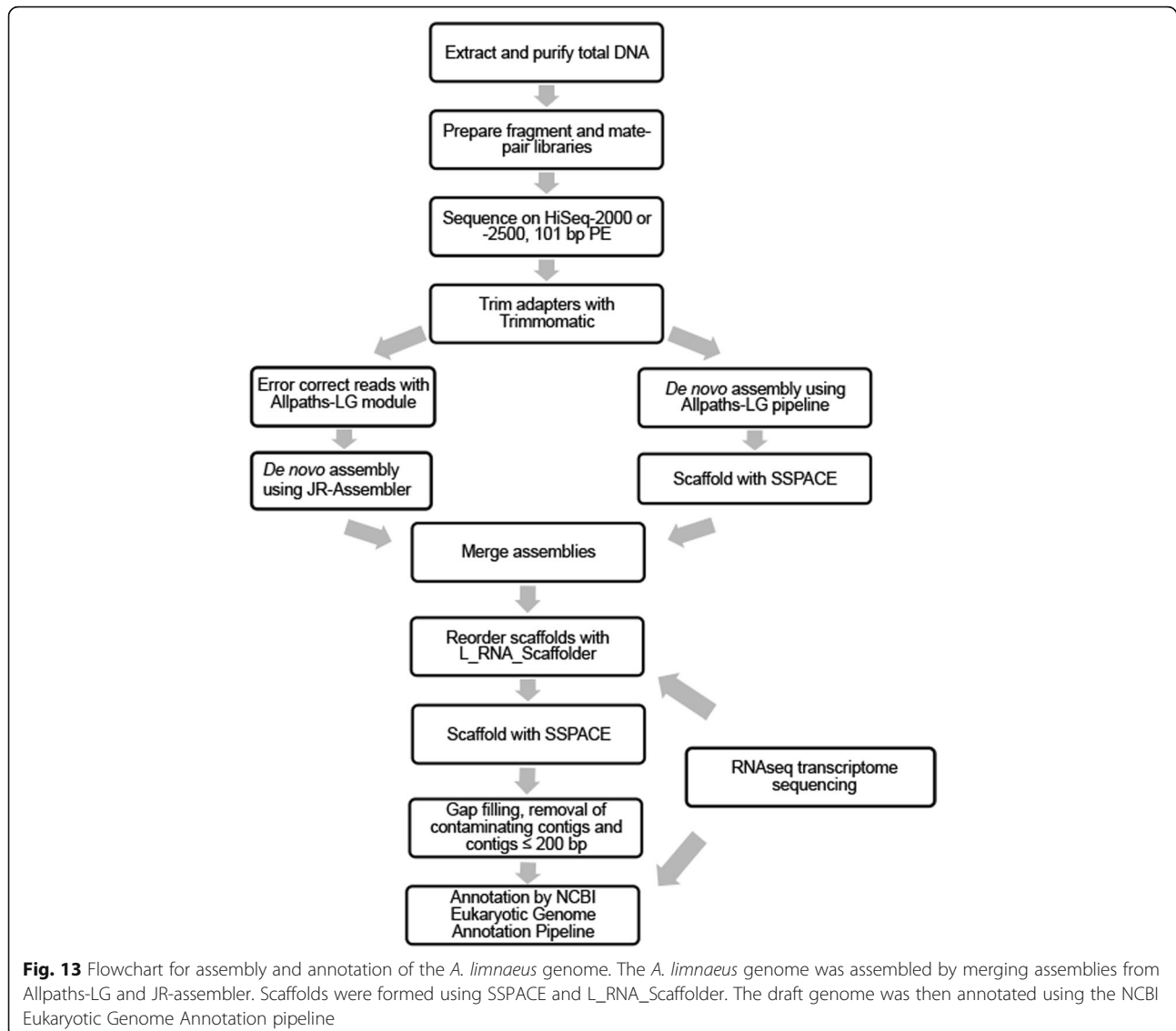
Fig. 13 Flowchart for assembly and annotation of the *A. limnaeus* genome. The *A. limnaeus* genome was assembled by merging assemblies from Allpaths-LG and JR-assembler. Scaffolds were formed using SSPACE and L_RNA_Scaffolder. The draft genome was then annotated using the NCBI Eukaryotic Genome Annotation pipeline

Wagner *et al. BMC Genomics* (2018) 19:155

Page 17 of 21

was used to improve the assembly by breaking apart and rejoining poorly supported scaffolds using a preliminary transcriptome derived from a 12 dpd embryo RNA-seq dataset (Riggs and Podrabsky, unpublished) [74]. The assembly was run through a final round of SSPACE Basic v3.0 and a custom script based on IMAGE (Tsai et al. 2010) was used to close gaps. The *Austrofundulus limnaeus* genome v1.0 has been screened and cleaned of contaminating contigs, and all contigs 200 bp or smaller were removed.

Automated annotation by NCBI

The NCBI eukaryotic annotation pipeline integrates ab initio gene modeling and protein/transcript/RNA-seq alignments to annotate genomes. The *A. limnaeus* genome v1.0 was submitted to NCBI and annotated using version 6.4 of this pipeline. A total of 114 RNA-seq biosamples (9,297,509,096 RNA-seq reads) from various treatments and stages of *A. limnaeus* embryonic development were obtained via SRA and used for gene prediction (Additional file 2: Table S2B).

Libraries of trimmed sequence reads (see methods below) grouped by stages and treatment were assembled de novo into transcriptome assemblies using Trinity software (version 2.0.6) [75], using a default k-mer length of 25 nucleotides (nts) for overlapping into contiguous sequences and the minimum contiguous sequence length setting (min_contig_length) at 200 nts. Assembled sequences have been deposited into the NCBI Transcriptome Shotgun Assembly (TSA) database with the TSA records listed in Additional file 2: Table S2C.

Analysis of genome assembly

Genome completeness of *Austrofundulus limnaeus* v1.0 was estimated with CEGMA version 2.5 on the CEGMA virtual machine v1.0 [76] http://korflab.ucdavis.edu/data-sets/cegma/cegma_vm.html). CEGMA scans genomic sequences for homologous sequences to 248 highly conserved eukaryotic genes. Genome completeness was also estimated with BUSCO version 1.22 using the vertebrata BUSCO profile [77]. BUSCO dependencies included AUGUSTUS v2.2.2, BLAST+ 2.2.28, and HMMER v3.1b2. Repetitive DNA elements in the *A. limnaeus* genome, such as transposons, were identified with RepeatModeler 1.0.8 [78].

Protein clustering analysis

Protein coding sequences (CDS) were downloaded from BioMart (Ensembl Genes release v82) or Genbank. CDS inferred from transcriptome assemblies were also used for several *Nothobranchius* species and one non-annual killifish species, *Aphyosemion striatum* (Additional file 1: Table S1A). CDS were

translated to amino acid sequences and only the longest isoform from each gene was retained for clustering analysis. Gene family clusters were inferred using Proteinortho v5.11 with default settings [79].

Phylogenetics

Genes identified as single-copy orthologs that were included in high-confidence clusters (Proteinortho Alg.-Conn score = 1) were aligned using MAFFT v7.158b and trimmed with GBLOCKS [80, 81]. The best-fit amino acid substitution model was determined using the resulting alignment as input to ProtTest 3.4.1 [82]. Phylogenetic inference using maximum-likelihood on this alignment was performed using PhyML v3.1 with the JTT + I + G protein substitution model and 100 bootstrap replications [83]. Based on findings by the Ensembl Compara team, our resulting tree was rooted by setting Zebrafish and Cavefish as outgroups (http://dec2016.archive.ensembl.org/info/about/speciestree.html).

Positive selection analysis

For positive selection analysis, we considered all gene clusters identified by Proteinortho that included an ortholog from *A. limnaeus*, *N. furzeri*, the non-annual killifish *A. striatum*, at least one other *Nothobranchius* species, and two other teleost fish (a minimum of six single copy genes from all the species). Coding sequences in the filtered clusters were aligned using PRANK v.140603 [84]. Poorly aligned regions were trimmed using GUIDANCE v2.0 [85]. Genes and individual amino acids under positive selection in the *A. limnaeus* lineage were then identified using the branch-site model in CODEML implemented in the Phylogenetic Analysis by Maximum Likelihood package (PAML) [86]. The phylogenetic tree generated using PhyML was used as the input guide tree (Fig. 2. To generate a high confidence list of genes and sites under possible positive selection in *A. limnaeus*, we considered genes that were (1) identified by PAML to have at least one site under selection along the *A. limnaeus* branch, (2) did not have gaps within ±5 amino-acids from the putatively selected sites, and (3) had an FDR-corrected *p*-value of less than 0.2 (< 20% FDR) for the sites. In our analysis, an FDR of 0.2 corresponded approximately to an uncorrected *P*-value of 0.01. We compared the resulting list of positively selected proteins in *A. limnaeus* to ones previously reported to be under positive selection in *N. furzeri* using an independently annotated genome [30]. To validate orthology between the two *N. furzeri* annotations and *A. limnaeus*, we performed an additional Proteinortho analysis that omitted the annual killifish transcriptomes but included both *N. furzeri* proteomes. This second Proteinortho output was then used to ensure

Wagner *et al. BMC Genomics* (2018) 19:155

Page 18 of 21

that the proteins reported to be under positive selection in the *N. furzeri* genome by Valenzano et al. [30] were in valid clusters that also contained expected orthologs of the NCBI annotated *N. furzeri* genome as well as *A. limnaeus*. Finally, *A. limnaeus* proteins that were also under putative positive selection in *N. furzeri* were used as input into InterProScan 5.24–63.0 (https://www.ebi.ac.uk/interpro/interproscan.html) to predict protein domains.

Embryo sampling and poly-A RNA sequencing

A. limnaeus embryos were collected from spawning adults according to previously established husbandry methods [35]. Embryos were maintained at 25 °C in darkness until DII [15, 17, 22]. For anoxia exposures, DII embryos were exposed to 24 h of anoxia at 25 °C in a Bactron III anaerobic chamber (Sheldon Manufacturing, Cornelius, OR) [87]. To obtain post-diapause II embryos, diapause was experimentally broken by exposing embryos to continuous light for 48 h at 30 °C. Embryos were then returned to 25 °C in darkness until staging at 4 days post diapause (dpd) [22]. For each treatment (DII normoxia, DII 24 h anoxia, and 4 dpd) four biological replicates ($n = 4$), comprised of 20 embryos each, were flash-frozen and stored at – 80 °C until RNA extraction. Total RNA was extracted using TRIzol reagent (Invitrogen Inc., Carlsbad, California) as previously described [88]. cDNA libraries were prepared using the Illumina TruSeq RNA Sample Preparation kit (v2, Illumina, San Diego, CA, USA) following the manufacturer's instructions with 1 μg of total RNA as starting material. The purified cDNA libraries were quantified by qPCR and their quality was confirmed by a 2100 Bioanalyzer (Agilent Technologies, Santa Clara, CA, USA) using a DNA 1000 chip. The libraries were sequenced (100 nt paired-end reads, 4 samples multiplexed per lane on the flow cell) on an Illumina HiSeq 2000 at Oregon Health & Science University.

Analysis of poly-a RNA sequence data

The following analyses were performed in a UNIX environment on the Portland State University computing cluster. Sequence quality was initially assessed using FastQC, version 0.10.1 [89] to ensure high quality data. Sequence reads were filtered on quality scores and trimmed for the presence of adapter sequences using Trimmomatic [71] with the settings "ILLUMINA-CLIP:2:30:7:1:true", "SLIDINGWINDOW:5:15", "LEADING:20", "TRAILING:20", and "MINLEN: 25". Quality reads were mapped to the *A. limnaeus* genome 1.0 using the *–very-fast-local* preset in Bowtie2 [90]. Preserved paired reads after trimming were aligned in paired-end mode and any orphaned mates after trimming were aligned in single-end mode. These data sets were deposited into the SRA with the accession numbers listed in

Additional file 2: Table S2D. Reads that aligned to the *A. limnaeus* nuclear and mitochondrial [44] genome with 0 mismatches were used for expression analyses. Transcript counts per gene (union mode) were generated for all samples using the *summarizeOverlaps* function of the GenomicAlignments package from Bioconductor [91] and the NCBI *A. limnaeus* Genome Annotation Release 100. Count matrices were filtered for genes with 1 or more normalized counts summed across all replicates. Gene abundances were calculated as FPKM and differential expression analysis was performed using DESeq2 in the R Bioconductor package. Differential gene expression was determined on gene count data using the negative binomial distribution and estimations of mean-variance dependence [92] using a Benjamini-Hochberg multiple comparisons adjusted FDR of 5%.

Gene ontology enrichment analysis

For differentially expressed genes and genes identified as being under possible positive selection in *A. limnaeus*, we inferred gene ontology (GO) terms using human orthologs. A BLASTp search against *A. limnaeus* proteins was run using human proteins obtained from Ensembl (Assembly GRCh38, Release 37). The top hit for each gene with a minimum e-value of 10^{-5} was used to infer orthology. GO terms for the orthologous genes were obtained using the online UniProt Retrieve/ID mapping tool. We used hypergeometric test implemented in the Bioconductor package GoStats [93] to determine GO term enrichment. For the genes under possible positive selection, we used all the filtered genes input into PAML as background. For RNA-seq, genes with an average FPKM of at least 2 in either of the groups being compared were used as background.

Additional files

Additional file 1: Spreadsheet containing **Tables S1A-J.** The spreadsheet contains supplemental information on the species used for clustering analysis, positive selection results, GO term enrichment results, differential transcript abundance results, and Hsp70 family transcript abundance results. (XLSX 997 kb)

Additional file 2: Spreadsheet containing **Tables S2A-D.** The spreadsheet contains information on the libraries used for assembly and annotation of the *A. limnaeus* genome. In addition, the spreadsheet contains information on the RNA-seq libraries used for differential expression analysis. (XLSX 65 kb)

Wagner *et al. BMC Genomics* (2018) 19:155

Page 19 of 21

Availability of data and materials
The *A. limnaeus* genome assembly is available on NCBI GenBank under accession GCA_001266775.1. The *A. limnaeus* genome annotation is available on NCBI Genome under NCBI *Austrofundulus limnaeus* Annotation Release 100. All raw reads and TSAs used in this study are available on NCBI and are listed in Additional file 1: Table S1A,B. The concatenated protein alignment used as input for tree building with PhyML has been uploaded to TreeBase (http://purl.org/phylo/treebase/phylows/study/TB2:S22058).

Authors' contributions
JW extracted and submitted DNA for sequencing, performed genome read quality control and assembly, performed scaffolding with SSPACE, performed CEGMA and BUSCO analyses, interpreted the PAML, GO term enrichment and RNA-seq results, performed the protein clustering with proteinortho, constructed the phylogenetic tree, performed the flow cytometry genome size estimate, and prepared the manuscript. SCW assisted with organizing the GO term enrichment results and summarizing the RNA-seq differential expression results. PPS performed the multiple species alignments and filtering with GBLOCKS and GUIDANCE, PAML positive selection analysis, GO term enrichment statistics, and provided the alignment for phylogenetic tree inference. JR assisted with summarizing and interpreting the hsp gene abundance data. ALR performed the RNA-seq differential expression bioinformatics and statistics. CLR performed the embryo anoxia treatments, collected and extracted total RNA from the embryos, and prepared the poly-A libraries for sequencing. ALR and CR prepared embryo RNA raw reads and Transcriptional Shotgun Assemblies (TSAs) for use in the NCBI Eukaryotic Annotation Pipeline. PM merged the two genome assemblies, removed genome assembly contamination, reordered the scaffolds using L_RNA_Scaffolder, performed RepeatModeler analysis, and assisted with submitting the assembled genome to NCBI Genbank for annotation. WW provided critical oversight of the assembly improvement steps. AB provided critical guidance and advice with the positive selection analysis. JEP provided manuscript and study advice, and conceived of the study with JW. All authors contributed writing to their respective sections and provided feedback for revisions on the manuscript. All authors read and approved the final manuscript.

Ethics approval and consent to participate
Austrofundulus limnaeus adults and embryos were maintained and sampled as approved by the Portland State University Institutional Animal Care and Use Committee (PSU protocol #33).

Consent for publication
Not applicable.

Competing interests
The authors declare that they have no competing interests.

Publisher's Note
Springer Nature remains neutral with regard to jurisdictional claims in published maps and institutional affiliations.

Author details
[1]Department of Biology, Center for Life in Extreme Environments, Portland State University, Portland, Oregon, USA. [2]Department of Genetics, Stanford University, Stanford, California, USA. [3]McDonnell Genome Institute at Washington University, St Louis, Missouri, USA. [4]Glenn Center for the Biology of Aging, Stanford, California, USA. [5]Knight Cancer Early Detection Advanced Research Center, Oregon Health and Science University, Portland, Oregon, USA.

References
1. Drinkwater LE, Clegg JS. Experimental biology of cyst diapause. In: Brown RA, Sorgeloos P, Trotman CNA, editors. Artemia Biology. Boca Raton: CRC Press, Inc.; 1991. p. 93–117.
2. Podrabsky JE, Hand SC. Physiological strategies during animal diapause: lessons from brine shrimp and annual killifish. J Exp Biol. 2015;218:1897–906.
3. Macrae TH. Diapause: diverse states of developmental and metabolic arrest. J Biol Res. 2005;3:3–14.
4. Clegg JS, Drinkwater LE, Sorgeloos P. The metabolic status of diapause embryos of *Artemia franciscana* (SFB). Physiol Zool. 1996;69(1):49–66.
5. Hand SC, Podrabsky JE. Bioenergetics of diapause and quiescence in aquatic animals. Thermochim Acta. 2000;349(1–2):31–42.
6. Clegg JS. Embryos of *Artemia franciscana* survive four years of continuous anoxia: the case for complete metabolic rate depression. J Exp Biol. 1997; 200(3):467–75.
7. Podrabsky JE, Hand SC. The bioenergetics of embryonic diapause in an annual killifish, *Austrofundulus limnaeus*. J Exp Biol. 1999;202(19):2567–80.
8. Hahn DA, Denlinger DL. Energetics of insect diapause. Annu Rev Entomol. 2011;56:103–21.
9. Podrabsky JE, Carpenter JF, Hand SC. Survival of water stress in annual fish embryos: dehydration avoidance and egg envelope amyloid fibers. Am J Phys. 2001;280(1):R123–31.
10. Machado BE, Podrabsky JE. Salinity tolerance in diapausing embryos of the annual killifish *Austrofundulus limnaeus* is supported by exceptionally low water and ion permeability. J Comp Physiol B. 2007;177(7):809–20.
11. Podrabsky JE, Lopez JP, Fan TWM, Higashi R, Somero GN. Extreme anoxia tolerance in embryos of the annual killifish *Austrofundulus limnaeus*: insights from a metabolomics analysis. J Exp Biol. 2007;210(13):2253–66.
12. Wagner JT, Podrabsky JE. Extreme tolerance and developmental buffering of UV-C induced DNA damage in embryos of the annual killifish *Austrofundulus limnaeus*. J Exp Zool. 2015;323A:10–30.
13. Podrabsky JE, Hrbek T, Physical HSC. Chemical characteristics of ephemeral pond habitats in the Maracaibo basin and llanos region of Venezuela. Hydrobiologia. 1998;362(1–3):67–78.
14. Myers GS. Annual fishes. Aquarium J. 1952;23:125–41.
15. Wourms JP. Developmental biology of annual fishes I. Stages in the normal development of *Austrofundulus myersi* dahl. J Exp Zool. 1972;182(2):143–68.
16. Wourms JP. The developmental biology of annual fishes II. Naturally occurring dispersion and reaggregation of blastomeres during the development of annual fish eggs. J Exp Zool. 1972;182:169–200.
17. Wourms JP. The developmental biology of annual fishes III. Pre-embryonic and embryonic diapause of variable duration in the eggs of annual fishes. J Exp Zool. 1972;182(3):389–414.
18. Lesseps R, Hall M, Murnane MB. Contact inhibition of cell movement in living embryos of an annual fish, *Nothobranchius korthausae*: its role in the switch from persistent to random cell movement. J Exp Zool. 1979;207:459–70.
19. Lesseps RJ, Lapeyre MV, Hall MV. Tissue culture evidence on the control of the switch from contact inhibition of cell movement to overlapping behavior in annual fish embryos of *Nothobranchius korthausae*. J Exp Zool. 1979;210(3):521–8.
20. Wagner JT, Podrabsky JE. Gene expression patterns that support novel developmental stress buffering in embryos of the annual killifish *Austrofundulus limnaeus*. EvoDevo. 2015;6:2.
21. Podrabsky J, Riggs C, Wagner J. Tolerance of Environmental Stress. In: Berois N, García G, De Sá R, editors. Annual Fishes Life History Strategy, Diversity, and Evolution. Boca Raton, FL USA: CRC Press, Taylor & Francis; 2016. p. 159–184.
22. Podrabsky J, Riggs C, Romney A, Woll S, Wagner J, Culpepper K, Cleaver T. Embryonic development of the annual killifish *Austrofundulus limnaeus*: an emerging model for ecological and evolutionary developmental biology research and instruction. Dev Dyn. 2017;246:779–801.
23. Podrabsky JE, Garrett IDF, Kohl ZF. Alternative developmental pathways associated with diapause regulated by temperature and maternal influences in embryos of the annual killifish *Austrofundulus limnaeus*. J Exp Biol. 2010; 213(19):3280–8.
24. Podrabsky J, Romney A, Culpepper K. Alternative Developmental Pathways. In: Berois N, García G, De Sá R, editors. Annual Fishes Life History Strategy,

Wagner *et al. BMC Genomics* (2018) 19:155

Page 20 of 21

Diversity, and Evolution. Boca Raton, FL USA: CRC Press, Taylor & Francis; 2016. p. 63–73.

25. Nilsson GE, Lutz PL. Anoxia tolerant brains. J Cereb Blood Flow Metab. 2004; 24(5):475–86.

26. Podrabsky JE, Riggs CL, Duerr JM. Anoxia tolerance during vertebrate development - insights from studies on the annual killifish *Austrofundulus limnaeus*. In: Padilla P, editor. Anoxia. Rijeka, Croatia: InTech; 2012. p. 3–24.

27. Meller CL, Meller R, Simon RP, Culpepper KM, Podrabsky JE. Cell cycle arrest associated with anoxia-induced quiescence, anoxic preconditioning, and embryonic diapause in embryos of the annual killifish *Austrofundulus limnaeus*. J Comp Physiol B. 2012;182:909–20.

28. Meller CL, Podrabsky JE. Avoidance of apoptosis in embryonic cells of the annual killifish *Austrofundulus limnaeus* exposed to anoxia. PLoS One. 2013; 8(9):e75837.

29. Podrabsky JE, Menze MA, Hand SC. Rapid Communication: Long-term survival of anoxia despite rapid ATP decline in embryos of the annual killifish *Austrofundulus limnaeus*. J Exp Zool A. 2012;317:524–32.

30. Valenzano DR, Benayoun BA, Singh PP, Zhang E, Etter PD, Hu C-K, Clément-Ziza M, Willemsen D, Cui R, Harel I. The African turquoise killifish genome provides insights into evolution and genetic architecture of lifespan. Cell. 2015;163(6):1539–54.

31. Reichwald K, Petzold A, Koch P, Downie BR, Hartmann N, Pietsch S, Baumgart M, Chalopin D, Felder M, Bens M. Insights into sex chromosome evolution and aging from the genome of a short-lived fish. Cell. 2015;163(6): 1527–38.

32. Hrbek T, Larson A. The evolution of diapause in the killifish family Rivulidae (Atherinomorpha, Cyprinodontiformes): a molecular phylogenetic and biogeographic perspective. Evolution. 1999;53(4):1200–16.

33. Furness AI. The evolution of an annual life cycle in killifish: adaptation to ephemeral aquatic environments through embryonic diapause. Biol Rev. 2016;91:796–812.

34. Furness AI, Reznick DN, Springer MS, Meredith RW. Convergent evolution of alternative developmental trajectories associated with diapause in African and South American killifish. Proc Roy Soc Lond B Bio. 2015;282:20142189.

35. Podrabsky JE. Husbandry of the annual killifish *Austrofundulus limnaeus* with special emphasis on the collection and rearing of embryos. Environ Biol Fish. 1999;54(4):421–31.

36. Gnerre S, MacCallum I, Przybylski D, Ribeiro FJ, Burton JN, Walker BJ, Sharpe T, Hall G, Shea TP, Sykes S. High-quality draft assemblies of mammalian genomes from massively parallel sequence data. Proc Natl Acad Sci U S A. 2011;108(4):1513–8.

37. Yao G, Ye L, Gao H, Minx P, Warren WC, Weinstock GM. Graph accordance of next-generation sequence assemblies. Bioinformatics. 2011;28(1):13–6.

38. Elder JF Jr, Turner BJ, Thomerson JE, Taphorn DC. Karyotypes of nine Venezuelan annual killifishes (Cyprinodontidae), with comments on karyotype differentiation in annual killifishes. Ichthyol Explor Freshwat. 1993; 4(3):261–8.

39. García G, Ríos N, Gutiérrez V. Next-generation sequencing detects repetitive elements expansion in giant genomes of annual killifish genus *Austrolebias* (Cyprinodontiformes, Rivulidae). Genetica. 2015;143(3):353–60.

40. Reichwald K, Lauber C, Nanda I, Kirschner J, Hartmann N, Schories S, Gausmann U, Taudien S, Schilhabel MB, Szafranski K, et al. High tandem repeat content in the genome of the short-lived annual fish *Nothobranchius furzeri*: a new vertebrate model for aging research. Genome Biol. 2009;10(2): R16.11–7.

41. Duerr JM, Podrabsky JE. Mitochondrial physiology of diapausing and developing embryos of the annual killifish *Austrofundulus limnaeus*: implications for extreme anoxia tolerance. J Comp Physiol B. 2010;180(7): 991–1003.

42. Sahm A, Bens M, Platzer M, Cellerino A. Parallel evolution of genes controlling mitonuclear balance in short-lived annual fishes. Aging Cell. 2017;16:488–96.

43. Hirst J. Mitochondrial complex I. Annu Rev Biochem. 2013;82:551–75.

44. Wagner J, Herrejon Chavez F, Podrabsky J. Mitochondrial DNA sequence and lack of response to anoxia in the annual killifish *Austrofundulus limnaeus*. Front Physiol. 2016;7:379.

45. Vinothkumar KR, Zhu J, Hirst J. Architecture of mammalian respiratory complex I. Nature. 2014;515(7525):80–4.

46. Stowe DF, Camara AK. Mitochondrial reactive oxygen species production in excitable cells: modulators of mitochondrial and cell function. Antioxid Redox Signal. 2009;11(6):1373–414.

47. Quinlan CL, Treberg JR, Perevoshchikova IV, Orr AL, Brand MD. Native rates of superoxide production from multiple sites in isolated mitochondria measured using endogenous reporters. Free Radic Biol Med 2012;53(9):1807–1817.

48. Milton SL, Nayak G, Kesaraju S, Kara L, Prentice HM. Suppression of reactive oxygen species production enhances neuronal survival in vitro and in vivo in the anoxia-tolerant turtle *Trachemys scripta*. J Neurochem. 2007;101(4):993–1001.

49. Bar-Yaacov D, Blumberg A, Mishmar D. Mitochondrial-nuclear co-evolution and its effects on OXPHOS activity and regulation. BBA-Gene Regul Mech. 2012;1819(9–10):1107–11.

50. Storey KB. Anoxia tolerance in turtles: metabolic regulation and gene expression. Comp Biochem Physiol A Mol Integr Physiol. 2007;147(2):263–76.

51. Hand SC. Quiescence in *Artemia franciscana* embryos: reversible arrest of metabolism and gene expression at low oxygen levels. J Exp Biol. 1998; 201(8):1233–42.

52. Hand SC, Hardewig I. Downregulation of cellular metabolism during environmental stress: mechanisms and implications. Annu Rev Physiol. 1996; 58:539–63.

53. Hightower LE, Norris CE, Di Iorio PJ, Fielding E. Heat shock responses of closely related species of tropical and desert fish. Am Zool. 1999;39(6): 877–88.

54. Norris CE, Brown MA, Hickey E, Weber LA, Hightower LE. Low-molecular-weight heat shock proteins in a desert fish (*Poeciliopsis lucida*): homologs of human Hsp27 and *Xenopus* Hsp30. Mol Biol Evol. 1997;14(10):1050–61.

55. Bai Y, Shakeley RM, Attardi G. Tight control of respiration by NADH dehydrogenase ND5 subunit gene expression in mouse mitochondria. Mol Cell Biol. 2000;20(3):805–15.

56. Chomyn A. Mitochondrial genetic control of assembly and function of complex I in mammalian cells. J Bioenerg Biomembr. 2001;33(3):251–7.

57. Piruat JI, López-Barneo J. Oxygen tension regulates mitochondrial DNA-encoded complex I gene expression. J Biol Chem. 2005;280(52):42676–84.

58. Montier LLC, Deng JJ, Bai Y. Number matters: control of mammalian mitochondrial DNA copy number. J Genet Genomics. 2009;36(3):125–31.

59. Rand DM, Haney RA, Fry AJ. Cytonuclear coevolution: the genomics of cooperation. Trends Ecol Evol. 2004;19(12):645–53.

60. Goldfarb SB, Kashlan OB, Watkins JN, Suaud L, Yan W, Kleyman TR, Rubenstein RC. Differential effects of Hsc70 and Hsp70 on the intracellular trafficking and functional expression of epithelial sodium channels. Proc Natl Acad Sci U S A. 2006;103(15):5817–22.

61. Okamoto K, Beach D. Cyclin G is a transcriptional target of the p53 tumor suppressor protein. EMBO J. 1994;13(20):4816.

62. Zhao L, Samuels T, Winckler S, Korgaonkar C, Tompkins V, Horne MC, Quelle DE. Cyclin G1 has growth inhibitory activity linked to the ARF-Mdm2-p53 and pRb tumor suppressor pathways. Mol Cancer Res. 2003;1(3):195–206.

63. Feder ME, Hofmann GE. Heat-shock proteins, molecular chaperones, and the stress response: evolutionary and ecological physiology. Annu Rev Physiol. 1999;61(1):243–82.

64. Mayer M, Bukau B. Hsp70 chaperones: cellular functions and molecular mechanism. Cell Mol Life Sci. 2005;62(6):670.

65. Pockley AG. Heat shock proteins as regulators of the immune response. Lancet. 2003;362(9382):469–76.

66. Podrabsky JE, Somero GN. An inducible 70 kDa-class heat shock protein is constitutively expressed during early development and diapause in the annual killifish *Austrofundulus limnaeus*. Cell Stress Chaperones. 2007;12(3): 199–204.

67. Lutz PL, Milton SL. Negotiating brain anoxia survival in the turtle. J Exp Biol. 2004;207(18):3141–7.

68. Heikkila JJ, Browder LW, Gedamu L, Nickells RW, Schultz GA. Heat-shock gene expression in animal embryonic systems. Can J Genet Cytol. 1986; 28(6):1093–105.

69. Krone PH, Sass JB, Lele Z. Heat shock protein gene expression during embryonic development of the zebrafish. Cell Mol Life Sci. 1997;53(1):122–9.

70. Lele Z, Engel S, Krone PH. *hsp47* and *hsp70* gene expression is differentially regulated in a stress- and tissue-specific manner in zebrafish embryos. Dev Genet. 1997;21(2):123–33.

71. Bolger AA, Lohse M, Usadel B. Trimmomatic: a flexible trimmer for Illumina sequence data. Bioinformatics. 2014;30(15):2114–20.

72. Chu T-C, Lu C-H, Liu T, Lee GC, Li W-H, Shih AC-C. Assembler for de novo assembly of large genomes. Proc Natl Acad Sci U S A. 2013; 110(36):E3417–24.

73. Boetzer M, Henkel CV, Jansen HJ, Butler D, Pirovano W. Scaffolding pre-assembled contigs using SSPACE. Bioinformatics. 2011;27(4):578–9.

Wagner *et al. BMC Genomics* (2018) 19:155

Page 21 of 21

74. Xue W, Li J-T, Zhu Y-P, Hou G-Y, Kong X-F, Kuang Y-Y, Sun X-W. L_RNA_scaffolder: scaffolding genomes with transcripts. BMC Genomics. 2013;14(1):604.

75. Grabherr MG, Haas BJ, Yassour M, Levin JZ, Thompson DA, Amit I, Adiconis X, Fan L, Raychowdhury R, Trinity ZQ. Reconstructing a full-length transcriptome without a genome from RNA-Seq data. Nat Biotech. 2011;29(7):644.

76. Parra G, Bradnam K, Korf I. CEGMA: a pipeline to accurately annotate core genes in eukaryotic genomes. Bioinformatics. 2007;23(9):1061–7.

77. Simão FA, Waterhouse RM, Ioannidis P, Kriventseva EV, Zdobnov EM. BUSCO: assessing genome assembly and annotation completeness with single-copy orthologs. Bioinformatics. 2015:btv351.

78. Smit A, Hubley R. RepeatModeler. Institute of Syst Biol. 2011;1(5)

79. Lechner M, Findeiß S, Steiner L, Marz M, Stadler PF, Prohaska SJ. Proteinortho: Detection of (co-) orthologs in large-scale analysis. BMC Bioinformatics. 2011;12(1):1.

80. Castresana J. Selection of conserved blocks from multiple alignments for their use in phylogenetic analysis. Mol Biol Evol. 2000;17(4):540–52.

81. Katoh K, Standley DM. MAFFT multiple sequence alignment software version 7: improvements in performance and usability. Mol Biol Evol. 2013;30(4):772–80.

82. Darriba D, Taboada GL, Doallo R, Posada D. ProtTest 3: fast selection of best-fit models of protein evolution. Bioinformatics. 2011;27(8):1164–5.

83. Guindon S, Dufayard J-F, Lefort V, Anisimova M, Hordijk W, Gascuel O. New algorithms and methods to estimate maximum-likelihood phylogenies: assessing the performance of PhyML 3.0. Syst Biol. 2010;59(3):307–21.

84. Löytynoja A, Goldman N. Phylogeny-aware gap placement prevents errors in sequence alignment and evolutionary analysis. Science. 2008;320(5883):1632–5.

85. Sela I, Ashkenazy H, Katoh K, Pupko T. GUIDANCE2: accurate detection of unreliable alignment regions accounting for the uncertainty of multiple parameters. Nucleic Acids Res. 2015;43(W1):W7–W14.

86. Yang Z. PAML 4: phylogenetic analysis by maximum likelihood. Mol Biol Evol. 2007;24(8):1586–91.

87. Riggs C, Podrabsky J. Small noncoding RNA expression during extreme anoxia tolerance of annual killifish (*Austrofundulus limnaeus*) embryos. Physiol Genomics. 2017;49(9):505–18.

88. Romney A, Podrabsky J. Transcriptomic analysis of maternally provisioned cues for phenotypic plasticity in the annual killifish, *Austrofundulus limnaeus*. EvoDevo. 2017;8:6.

89. Andrews S. FastQC: a quality control tool for high throughput sequence data. 2010. https://www.bioinformatics.babraham.ac.uk/projects/fastqc/.

90. Langmead B, Salzberg SL. Fast gapped-read alignment with bowtie 2. Nat Methods. 2012;9(4):357–9.

91. Gentleman RC, Carey VJ, Bates DM, Bolstad B, Dettling M, Dudoit S, Ellis B, Gautier L, Ge Y, Gentry J, et al. Bioconductor: open software development for computational biology and bioinformatics. Genome Biol. 2004;5(10):R80.

92. Love MI, Huber W, Anders S. Moderated estimation of fold change and dispersion for RNA-seq data with DESeq2. Genome Biol. 2014;15:550.

93. Falcon S, Gentleman R. Using GOstats to test gene lists for GO term association. Bioinformatics. 2006;23(2):257–8.

94. Howe K, Clark MD, Torroja CF, Torrance J, Berthelot C, Muffato M, Collins JE, Humphray S, McLaren K, Matthews L. The zebrafish reference genome sequence and its relationship to the human genome. Nature. 2013;496(7446):498–503.

95. Jones FC, Grabherr MG, Chan YF, Russell P, Mauceli E, Johnson J, Swofford R, Pirun M, Zody MC, White S. The genomic basis of adaptive evolution in threespine sticklebacks. Nature. 2012;484(7392):55–61.

96. Star B, Nederbragt AJ, Jentoft S, Grimholt U, Malmstrøm M, Gregers TF, Rounge TB, Paulsen J, Solbakken MH, Sharma A. The genome sequence of Atlantic cod reveals a unique immune system. Nature. 2011;477(7363):207–10.

97. Romiguier J, Ranwez V, Douzery EJ, Galtier N. Contrasting GC-content dynamics across 33 mammalian genomes: relationship with life-history traits and chromosome sizes. Genome Res. 2010;20(8):1001–9.

98. de Koning AJ, Gu W, Castoe TA, Batzer MA, Pollock DD. Repetitive elements may comprise over two-thirds of the human genome. PLoS Genet. 2011;7(12):e1002384.

99. Kelley JL, Yee M-C, Brown AP, Richardson RR, Tatarenkov A, Lee CC, Harkins TT, Bustamante CD, Earley RL. The genome of the self-fertilizing mangrove rivulus fish, *Kryptolebias marmoratus*: a model for studying phenotypic plasticity and adaptations to extreme environments. Genome Biol Evol. 2016;8(7):2145–54.